Phosphatidylinositol 4-kinase IIβ negatively regulates invadopodia formation and suppresses an invasive cellular phenotype

Ganiyu Olabanji Alli-Balogun[a], Christina A. Gewinner[b], Ruth Jacobs[a], Janos Kriston-Vizi[c], Mark G. Waugh[a], and Shane Minogue[a,*]

[a]Lipid and Membrane Biology Group, UCL Division of Medicine, Royal Free Campus, University College London, London NW3 2PF, United Kingdom; [b]UCL Translational Research Office, London W1T 7JA, United Kingdom; [c]MRC Laboratory for Molecular Cell Biology, University College London, London WC1E 6BT, United Kingdom

ABSTRACT **The type II phosphatidylinositol 4-kinase (PI4KII) enzymes synthesize the lipid phosphatidylinositol 4-phosphate (PI(4)P), which has been detected at the Golgi complex and endosomal compartments and recruits clathrin adaptors. Despite common mechanistic similarities between the isoforms, the extent of their redundancy is unclear. We found that depletion of PI4KIIα and PI4KIIβ using small interfering RNA led to actin remodeling. Depletion of PI4KIIβ also induced the formation of invadopodia containing membrane type I matrix metalloproteinase (MT1-MMP). Depletion of PI4KII isoforms also differentially affected *trans*-Golgi network (TGN) pools of PI(4)P and post-TGN traffic. PI4KIIβ depletion caused increased MT1-MMP trafficking to invasive structures at the plasma membrane and was accompanied by reduced colocalization of MT1-MMP with membranes containing the endosomal markers Rab5 and Rab7 but increased localization with the exocytic Rab8. Depletion of PI4KIIβ was sufficient to confer an aggressive invasive phenotype on minimally invasive HeLa and MCF-7 cell lines. Mining oncogenomic databases revealed that loss of the PI4K2B allele and underexpression of PI4KIIβ mRNA are associated with human cancers. This finding supports the cell data and suggests that PI4KIIβ may be a clinically significant suppressor of invasion. We propose that PI4KIIβ synthesizes a pool of PI(4)P that maintains MT1-MMP traffic in the degradative pathway and suppresses the formation of invadopodia.**

Monitoring Editor
Benjamin S. Glick
University of Chicago

Received: Aug 2, 2016
Revised: Oct 5, 2016
Accepted: Oct 18, 2016

INTRODUCTION

The two human type II phosphatidylinositol 4-kinase (PI4KII) enzymes display 68% sequence identity across their conserved catalytic domains and exist in multiple subcellular membrane compartments (Balla and Balla, 2006; Minogue and Waugh, 2012). Since the molecular characterization of the PI4KIIs, a general model of PI4KII function in post–*trans*-Golgi network (TGN) traffic has gradually emerged in which the kinases generate phosphatidylinositol 4-phosphate (PI(4)P), which is required for the recruitment of clathrin adaptors needed in TGN-to-endosomal traffic. PI4KIIs have been most extensively described in endosomes (Balla *et al.*, 2002), the TGN (Wang *et al.*, 2003), and at the plasma membrane (Minogue *et al.*, 2006), as has PI(4)P (Hammond *et al.*, 2014). The PI4KIIα isoform generates PI(4)P, which interacts with AP-1 (Wang *et al.*, 2003), GGAs (Wang *et al.*, 2007), and AP-3 (Salazar *et al.*, 2005; Craige *et al.*, 2008; Mossinger *et al.*, 2012) and therefore has roles in TGN-to-endosome and TGN-to–late endosomal trafficking known to be important in transport to the lysosome. More recently, a mechanism has been described involving the redirection of PI from phosphatidylinositol 3-phosphate (PI(3)P) into PI(4)P synthesis, which is required for exocytic traffic from endosomes. This pathway requires PI4KIIα and is significant because it represents an important step in

This article was published online ahead of print in MBoC in Press (http://www.molbiolcell.org/cgi/doi/10.1091/mbc.E16-08-0564) on October 26, 2016.

S.M. and G.O.A. conceived and designed experiments and analyzed the data. S.M., G.O.A., C.A.G., and R.J. performed experiments. J.K. analyzed data. S.M., G.O.A., and M.G.W. drafted the article.

*Address correspondence to: Shane Minogue (s.minogue@ucl.ac.uk).

Abbreviations used: CI-M6PR, cation-independent mannose 6-phosphate receptor; CNA, copy number alteration; ECM, extracellular matrix; EE, early endosome; EEA1, early endosomal autoantigen 1; EGFR, epidermal growth factor receptor; GFP, green fluorescent protein; GST, glutathione-*S*-transferase; LE, late endosome; MT1-MMP, membrane type I matrix metalloproteinase; NT, nontargeting siRNA; P4C, PI(4)P-binding domain of SidC; PI4KIIα, phosphatidylinositol 4-kinase type II alpha; PI4KIIβ, phosphatidylinositol 4-kinase type II beta; PI(3)P, phosphatidylinositol 3-phosphate; PI(4)P, phosphatidylinositol 4-phosphate.

Supplemental Material can be found at:
http://www.molbiolcell.org/content/suppl/2016/10/24/mbc.E16-08-0564v1.DC1.html

the recycling of plasma membrane cargoes such as β1-integrin and the transferrin receptor (Ketel *et al.*, 2016). PI4KIIα has also been implicated in human cancer (Li *et al.*, 2010, 2014). PI4KIIβ functions in TGN-to-endosomal traffic by directly interacting with AP-1, playing a role in developmental signaling by controlling the endosomal traffic of Frizzled, a receptor for Wnt (Wieffer *et al.*, 2013). The PI4KII isoforms therefore produce lipids needed for different steps in post-TGN trafficking.

Protease-dependent matrix remodeling performs key physiological functions during embryo development and in the pathogenesis of metastatic disease. In metastatic cells, proteolytic degradation of extracellular matrix (ECM) is mediated by extracellular proteases such as the membrane type I metalloproteinase (MT1-MMP), whose increased expression is associated with a poor prognosis in a wide variety of human tumors (Egeblad and Werb, 2002). ECM invasion by tumor-derived cells is mediated in part by specialized actin- and phosphotyrosine-rich protrusions termed invadopodia, which are capable of degrading extracellular matrix through the directed membrane traffic of MMPs (Poincloux *et al.*, 2009). The overexpression of components of invadopodia such as cortactin in breast and squamous carcinomas and ovarian, bladder, and lung cancers is associated with a more aggressive phenotype and poorer patient prognosis (Paz *et al.*, 2014). MT1-MMP is a key component of mature invadopodia and has been implicated in breaching of basement membranes and invasion through interstitial collagen (Sabeh *et al.*, 2004; Hotary *et al.*, 2006). Trafficking to the plasma membrane from endosomal compartments is a recognized pathway for the delivery of MT1-MMP to invadopodia (Steffen *et al.*, 2008; Yu *et al.*, 2012). However, the molecular machinery controlling the complex trafficking of this key protease is not fully understood.

The PI4KII enzymes have been associated with both the development of breast cancer (Li *et al.*, 2014) and metastasis of hepatocellular carcinoma (HCC; Mazzocca *et al.*, 2008), but links between the PI4KIIs and cellular processes such as actin reorganization during oncogenesis are unclear. We therefore investigated the role of PI4KIIα and PI4KIIβ in actin remodeling and found that depletion of the enzymes had starkly different effects on the actin cytoskeleton. We also found that PI4KIIβ depletion specifically induced the formation of invadopodia and was sufficient to convert HeLa and MCF-7 cells into an invasive phenotype. Loss of PI4KIIα and PI4KIIβ affected different PI(4)P TGN pools and post-TGN traffic. The steady-state distribution of MT1-MMP was also shifted from an endosomal to an exocytic trafficking route. Finally, database analyses indicated that PI4KIIβ was lost in human cancers, indicating that PI4KIIβ may be a clinically significant tumor suppressor.

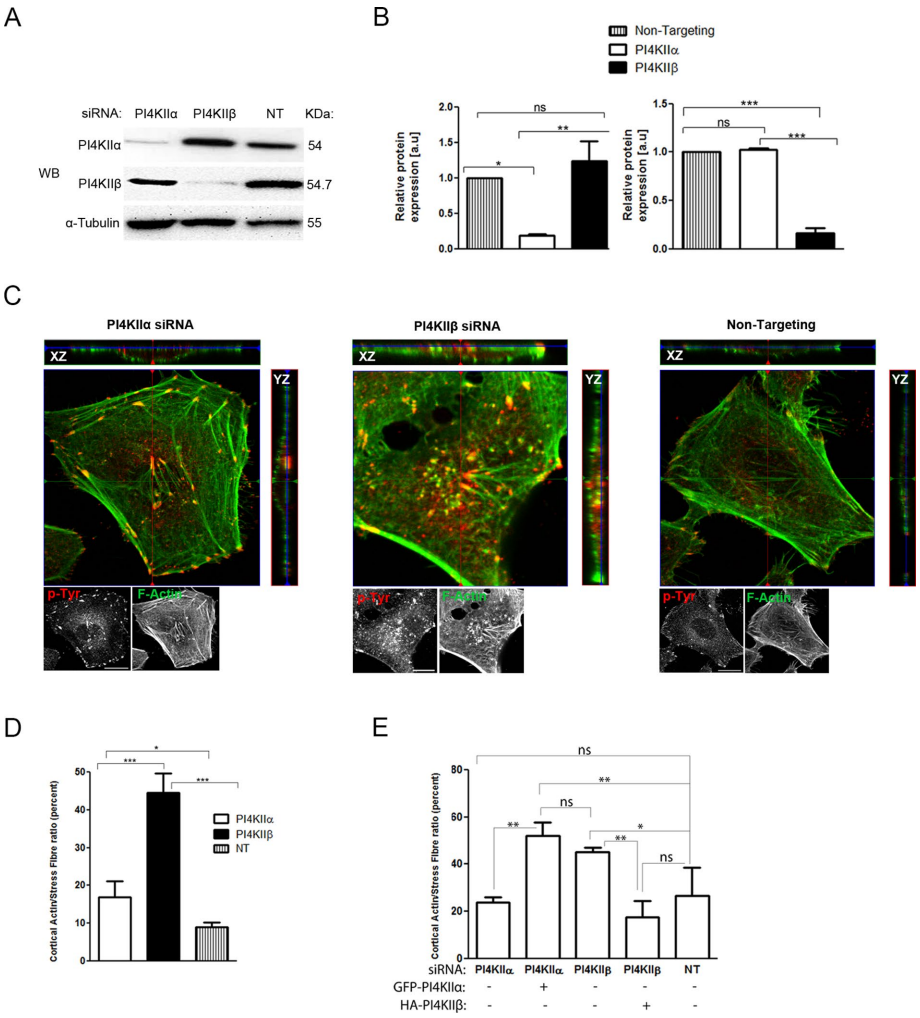

FIGURE 1: PI4KIIα and PI4KIIβ exert different effects on the actin cytoskeleton. (A, B) Total cell lysates of PI4KIIα, PI4KIIβ, and control siRNA-transfected HeLa cells were analyzed for protein expression by Western blotting; α-tubulin served as a control for protein levels. (C) HeLa cells transfected with the siRNA SMARTpool as indicated for 36 h were reseeded onto collagen matrix and then costained for tyrosine phosphorylated proteins (red) and the actin cytoskeleton (green). Confocal sections were acquired at 0.25-μm intervals and rendered into orthogonal views. Single *XY*-sections of the basal surface. Single pY and F-actin channels are shown below. Scale bars, 10 μm. (D) Ratio of cortical actin to stress fiber intensity from three independent experiments ($n = 20$ cells). (E) Cells were also transfected with single siRNA oligos and rescued by reexpression of siRNA-resistant PI4KIIα and PI4KIIβ. Data are presented as mean ± SEM, $*p < 0.05$, $**p < 0.01$, $***p < 0.001$; ns, not significant.

RESULTS

Depletion of PI4KII isoforms differentially affects the actin cytoskeleton

We used small interfering RNA (siRNA) to induce loss of PI4KII function. Gene silencing was confirmed by immunoblotting 72 h after transfection of HeLa cells with isoform-specific siRNA SMARTpools. We repeatedly achieved at least 85% reduction in levels of PI4KIIα and PI4KIIβ compared with nontargeted controls (Figure 1, A and B, and Supplemental Figure S1, A and B). When we specifically depleted PI4KII isoforms in this way, we noted that monolayers of cells treated with PI4KIIβ siRNA were more dispersed than with PI4KIIα and controls (unpublished results), as described previously (Mazzocca *et al.*, 2008). To investigate this further, we stained the actin cytoskeleton with fluorescently labeled phalloidin and found that, in comparison to controls, loss of PI4KIIα led to increased actin stress fiber formation at leading

edges (Figure 1C). Cells also showed some clear focal colocalization with phosphotyrosine (Figure 1C). Loss of PI4KIIβ, on the other hand, resulted in complete loss of actin stress fibers and increased the intensity of cortical actin staining (Figure 1C), as well as of the formation of scattered, actin-rich punctae staining positive for phosphotyrosine (Figure 1C), which were absent in PI4KIIα and control siRNAs. Actin remodeling was confirmed by analyzing the ratio of cortical actin:stress fiber signals (Figure 1D), and normal actin phenotypes were restored by reexpression of siRNA-resistant PI4KIIβ (Figure 1E and Supplemental Figure S1, C–F). The same rescue experiment with overexpressed GFP-PI4KIIα led to increased levels of cortical actin (Figure 1E), a likely consequence of increasing PI(4)P levels (Henmi *et al.*, 2016), which would be expected to alter the actin cytoskeleton. These data indicate that loss of PI4KIIα and PI4KIIβ has markedly different effects on the actin cytoskeleton.

Loss of PI4KIIβ induces the formation of invadopodia

We sought to confirm the identity of the scattered actin-rich punctae in Figure 1C formed as a result of loss of PI4KIIβ. Initially, we costained F-actin along with the early endosomal marker EEA1; however, these showed minimal colocalization (Supplemental Figure S2A), indicating that these punctae were distinct from actin comets localized to endosomal membranes (Taunton *et al.*, 2000). Furthermore, these structures typically had average diameters of ≤0.25 μm, mostly clustered in regions under the nucleus, and were thus suggestive of invadopodia (Garcia *et al.*, 2014). To confirm the identity of these punctae, we immunostained cells for actin and cortactin, the coincidence of which is diagnostic of invadopodia and related structures (Garcia *et al.*, 2014).

We found that loss of PI4KIIβ, but not of PI4KIIα, induced the formation of punctae staining positive for both markers in HeLa cells (Figure 2A). When we acquired confocal *z*-series data from PI4KIIβ-depleted cells, we observed the colocalization of actin and cortactin at the ventral surface of gelatin-coated coverslips (Figure 2B), thereby confirming that these structures were indeed invadopodia. As further confirmation, we performed a positive control by treating cells with the phorbol ester phorbol-12-myristate-13-acetate (PMA; Tatin *et al.*, 2006) and found that the actin- and cortactin-rich structures were indistinguishable from those obtained by depletion of PI4KIIβ (Figure 2B). Key constituents of invadopodia are the matrix metalloproteinase MT1-MMP (Poincloux *et al.*, 2009) and β1-integrin (Destaing *et al.*, 2010). To determine whether the ventral structures contained known components of mature invadopodia, we stained siRNA-treated cells plated on coverslips coated with a three-dimensional (3D) layer of collagen for MT1-MMP and β1-integrin or cortactin. Confocal microscopy demonstrated the colocalization of these markers with MT1-MMP (Figure 2, C and D), particularly on the ventral surface of PI4KIIβ-depleted cells (Figure 2, E and F). Furthermore, these structures were seen to penetrate the 3D ECM when we performed *Z*-series confocal microscopy (Figure 2, E and F).

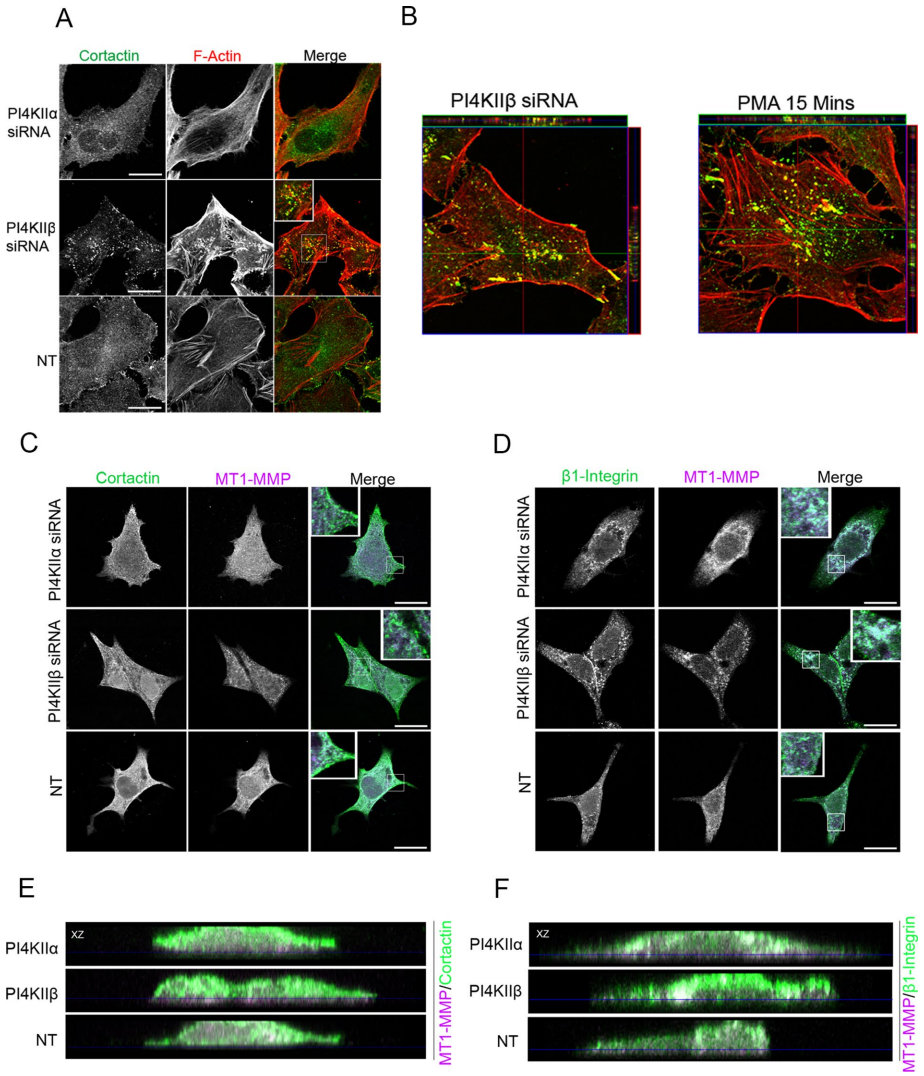

FIGURE 2: Depletion of PI4KIIβ induces invadopodia formation. (A) Confocal images showing immunostaining of cortactin (green) and F-actin (red). (B) Confocal images showing comparisons between HeLa cells transfected with PI4KIIβ siRNA and cells treated with 50 nM PMA. (C–F) Confocal images showing cells grown on thick layers of collagen and coimmunostained for MT1-MMP (magenta), (C) cortactin (green), or (D) β1-integrin (green). (E, F) *XZ* rendering of 20 confocal sections acquired at 0.25-μm intervals, showing localization of MT1-MMP to ventral structures containing cortactin (E) or β1-Integrin (F). Horizontal lines indicate the position of the ECM surface. Scale bars, 20 μm.

Loss of PI4KIIβ causes increased matrix degradation and migration through collagen gel

MT1-MMP requires posttranslational processing to become active (Williams and Coppolino, 2011). We therefore determined whether the structures formed upon the loss of PI4KIIβ expression were capable of ECM degradation. We plated target and control siRNA-transfected HeLa cells on an ECM composed of cross-linked fluorescein isothiocyanate (FITC)–conjugated gelatin. In comparison with PI4KIIα and control siRNA–transfected cells, loss of PI4KIIβ resulted in an approximately fourfold increase in fluorescent matrix degradation in comparison with PI4KIIα (Figure 3, A and B). Areas of degradation also

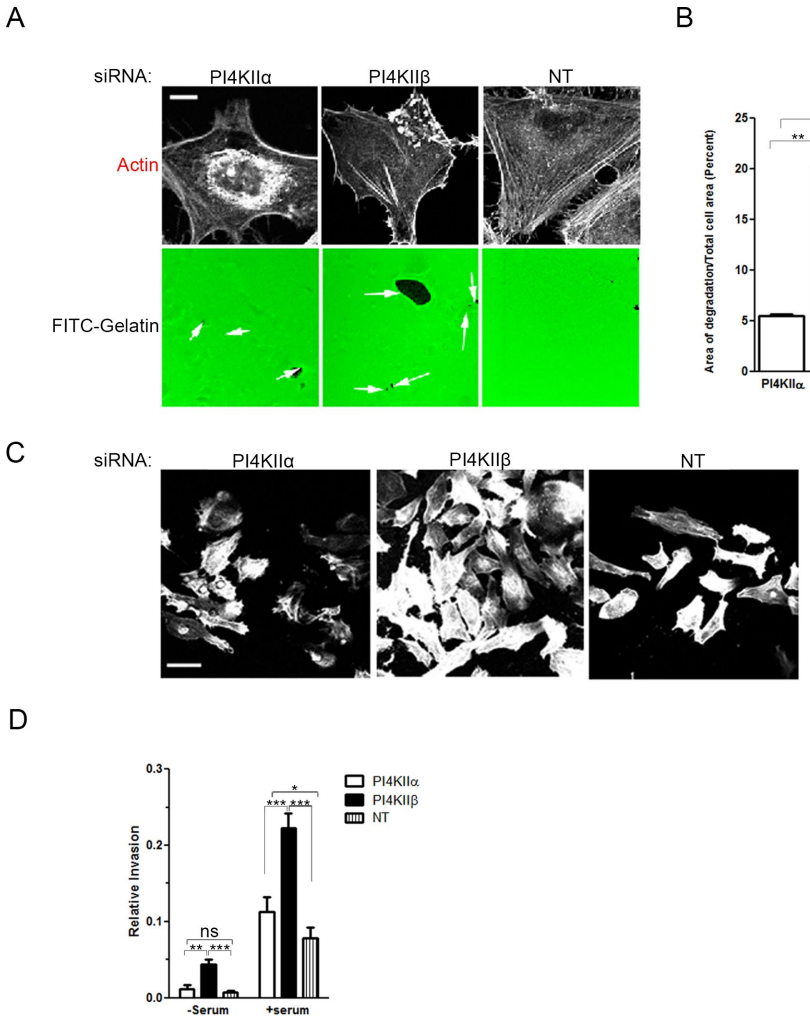

FIGURE 3: PI4KIIβ knockdown promotes ECM degradation and cell migration. (A) HeLa cells were reseeded onto FITC-gelatin–coated coverslips at 58 h posttransfection and then labeled for F-actin (red). Areas of proteolytic degradation are marked with arrows. (B) Percentage areas of degradation per total cell area in a 4×10^4 μm^2 field. Data are mean ± SEM ($n = 30$; experiment performed in triplicate). (C, D) HeLa cells were reseeded onto Transwell inserts coated with type I collagen gel (100 μl of 2 mg/ml) 58 h posttransfection and then placed in a chemoattractant (10% FCS) for 12 h. (C) Representative fields of cells that traversed the collagen-coated membrane of a Transwell chamber in response to chemoattractant. (D) Quantitation of invasion expressed as the ratio of cells that migrated toward chemoattractant relative to the total number of cells seeded onto the serum-free upper chamber. Data are presented as mean ± SEM, *$p < 0.05$, **$p < 0.01$, ***$p < 0.001$; ns, not significant.

corresponded to clusters of actin-rich punctae (Figure 3A), demonstrating that they were the source of the gelatinolytic activity.

We also performed Transwell invasion assays to measure the ability of PI4KII-depleted cells to invade a 3D collagen matrix in response to chemoattractant (serum). Invasion in the absence of serum was relatively low but significantly higher in PI4KIIβ siRNA cells. The introduction of serum to the lower chamber increased the number of migrating cells, with PI4KIIβ cells invading at approximately three times control values and two times that recorded for PI4KIIα-depleted cells (Figure 3, C and D, and Supplemental Figure S2B).

PI4KIIα and PI4KIIβ isoforms synthesize separate pools of TGN PI(4)P involved in TGN-to-endosome traffic

PI4KII isoforms are not known to directly influence the actin cytoskeleton; instead, they control trafficking from the TGN to endosomes through the recruitment of clathrin adaptors. To address the question of how PI4KIIβ knockdown leads to increased matrix degradation, we asked whether the PI4KII isoforms synthesized separate pools of PI(4)P and whether loss of this PI(4)P affected post-TGN membrane traffic. We visualized the PI(4)P generated by each PI4KII isoform by inhibiting PI4KIII activities with wortmannin in control and siRNA-treated cells. When we stained siRNA-treated cells with the PI(4)P reporter glutathione *S*-transferase (GST)–FAPP-PH, we noted that the intensity of staining in the Golgi region was affected in both PI4KIIα- and PI4KIIβ-knockdown cells but included signal from PI(4)P synthesized by the Golgi enzyme PI4KIIIβ (Supplemental Figure S3A). We therefore treated the same cells with wortmannin to inhibit PI4KIIIβ and fixed and stained the cells with recombinant GST-P4C, which is an unbiased PI(4)P reporter (Luo *et al.*, 2015). The residual GST-P4C signal allowed us to report the PI(4)P derived from the activity of PI4KIIα (PI(4)$P^{PI4KII\alpha}$) and PI4KIIβ (PI(4)$P^{PI4KII\beta}$; Figure 4, A–C, and Supplemental Figure S4D), which in both cases localized to membranes in the Golgi region and on cytoplasmic vesicles (Figure 4, A–C). Cells in which PI4KIIα was depleted showed residual PI(4)$P^{PI4KII\beta}$ staining that colocalized with TGN46 (Figure 4, A and D). In contrast, PI(4)$P^{PI4KII\alpha}$ predominantly colocalized with the TGN marker syntaxin 6 (Figure 4, B and D). Colocalization of PI(4)P with syntaxin 6 and TGN46 was restored upon expression of plasmids containing silent mutations rendering them resistant to siRNA (Figure 4, E and F, and Supplemental Figure S3, E and F). This demonstrates that the wortmannin-insensitive PI(4)$P^{PI4KII\alpha}$ and PI(4)$P^{PI4KII\beta}$ pools generated by the PI4KIIs exist in distinct subdomains of TGN/endosomal membranes and that knockdown of each isoform affects a metabolically separate PI(4)P compartment.

PI(4)P at the TGN is known to control the recruitment of the clathrin adaptor AP-1 in TGN-to-endosomal traffic (Wang *et al.*, 2003; Wieffer *et al.*, 2013), and we therefore reasoned that loss of TGN PI(4)P would affect this trafficking route. We investigated how loss of TGN PI(4)P altered the steady-state distribution of the cation-independent mannose-6-phosphate receptor (CI-M6PR), finding that PI4KIIα and PI4KIIβ led to a significant loss in colocalization between PI(4)P and this AP-1 cargo (Figure 4, C and D). This effect was particularly marked in PI4KIIβ cells, which also displayed a more compact staining pattern in the Golgi region and an absence of vesicular M6PR (Figure 4C). We also stained cells transfected with GFP-M6PR for AP-1 and found that PI4KIIβ siRNA cells showed reduced colocalization between them (Figure 4, G and H), indicating defective TGN-to-endosomal traffic. We tested the consequences on endolysosomal traffic by performing an epidermal growth factor receptor (EGFR) degradation assay and found that depletion of both PI4KIIα and

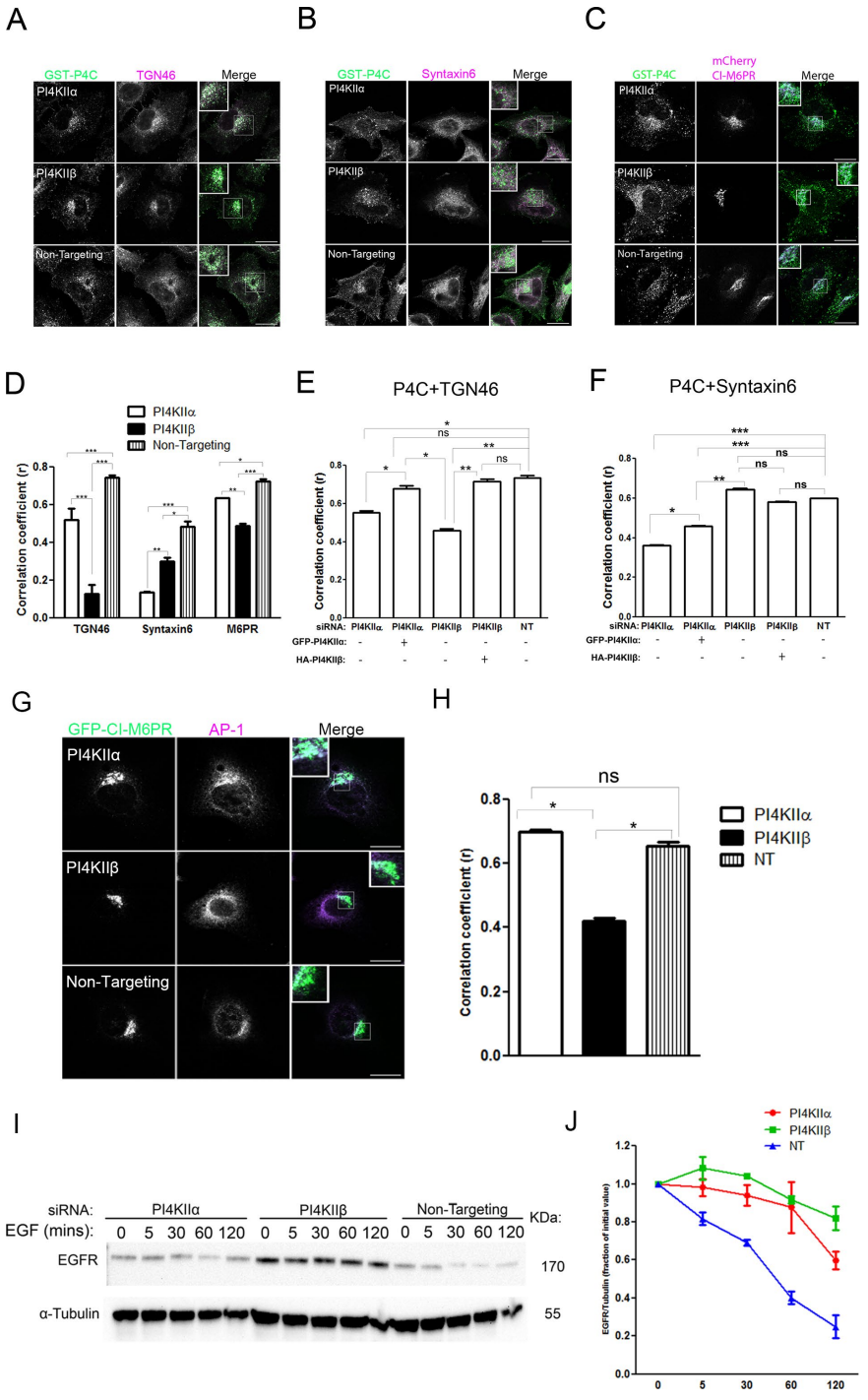

FIGURE 4: PI4KIIα and PI4KIIβ siRNA affects separate pools of PI(4)P at the TGN and perturbs TGN-endosomal traffic. (A–C) Recombinant GST-tagged protein containing the P4C domain from the *Legionella pneumoniae* SidC gene (GST-P4C) was used to indirectly stain membrane pools of PI(4)P after wortmannin treatment. Samples were costained with (A) TGN46 or (B) syntaxin 6 or (C) transfected with mCherry-tagged (CI-M6PR). (D) Pearson's *r* calculated for colocalization between PI(4)P and different TGN markers (20 cells, three independent experiments). (E, F) Pearson's *r* for colocalization between PI(4)P and (E) TGN46 or (F) syntaxin 6 after siRNA-mediated silencing with or without subsequent transfection with siRNA-resistant constructs. (G) Confocal images showing immunostaining for GFP-tagged CI-M6PR and adaptor AP-1. Scale bars, 10 μm. (H) Pearson's *r* for colocalized pixel intensities between the green (GFP) and magenta (AP-1) channels (20 cells, three independent experiments). (I) HeLa cells were transfected with the indicated siRNA oligos and then serum starved and stimulated with 100 ng/ml EGF for indicated times before analysis of EGFR levels by Western blotting. (J) Signal intensities were quantified by densitometry. Data are mean ± SEM ($n = 3$; three independent experiments). *$p < 0.05$, **$p < 0.01$, ***$p < 0.001$; ns, not significant.

PI4KIIβ significantly impaired ligand-induced degradation of the EGFR (Figure 4, I and J). Given that loss of either PI4KII isoform impairs EGFR degradation, we coimmunostained MT1-MMP with the lysosomal marker CD63 and found that both PI4KIIα and PI4KIIβ siRNA resulted in reduced colocalization (Supplemental Figure S4, A and B). Collectively these results show that loss of either PI(4)P pool affects TGN-to-endosome traffic and ultimately the degradation of cargo destined for lysosomes.

Loss of PI4KIIβ leads to increased exocytic trafficking of MT1-MMP

MT1-MMP is delivered to invadopodia from endosomal compartments (Steffen *et al.*, 2008; Wiesner *et al.*, 2013). We therefore considered that altered intracellular traffic might play a role in the increased localization of MT1-MMP to invadopodia. We analyzed cell surface MT1-MMP staining versus total cellular MT1-MMP using fluorescence-activated cell sorting (FACS) and found that loss of either PI4KII isoform led to an increase in total cellular MT1-MMP levels compared with controls (Supplemental Figure S4C); however, loss of PI4KIIβ led to an approximately threefold increase in MT1-MMP at the cell surface compared with control and PI4KIIα siRNA-transfected cells (Figure 5A).

Increased surface MT1-MMP could result from a decreased rate of endocytosis or an increased rate of exocytic trafficking. We therefore analyzed changes to the complex trafficking itinerary of MT1-MMP by coimmunostaining MT1-MMP and a selective panel of Rab GTPases known to control traffic of cargo in endosomal and Golgi membranes (Wiesner *et al.*, 2013). On loss of PI4KIIα and PI4KIIβ, MT1-MMP displayed decreased colocalization with early endosomal Rab5 and the late endosomal Rab7 (Figure 5, B and C). A significant increase in colocalization was observed with the post-Golgi Rab8, but meaningful differences were not detected in the colocalization of MT1-MMP with late endosomal Rab9 or the recycling endosomal Rab11 (Figure 5, B and C). This analysis demonstrates that MT1-MMP trafficking is redirected from an early endosomal (EE)–late endosomal (LE) route to the plasma membrane via a Rab8 exocytic route.

Loss of PI4KIIβ confers invasiveness on MCF-7 cells

We asked whether PI4KIIβ depletion was sufficient to convert the minimally invasive MCF-7 epithelial cell line into an invasive migratory phenotype. To test this, we evaluated the ability of PI4KIIβ-depleted MCF-7 cells

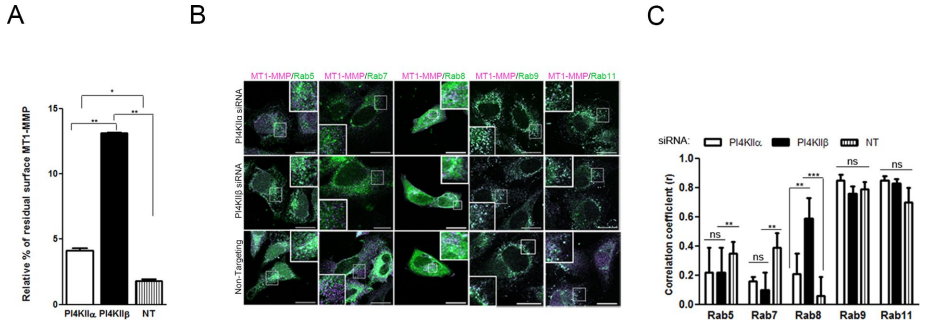

FIGURE 5: PI4KIIβ depletion alters trafficking of MT1-MMP. (A) Surface-labeled and total MT1-MMP were analyzed using flow cytometry, and the relative percentage of MT1-MMP present on the cell surface versus total cellular MT1-MMP was calculated. (B) Confocal immunofluorescence images showing MT1-MMP (magenta) and the indicated Rab GTPases (green). (C) Pearson's *r* for colocalization of MT1-MMP and the indicated Rab GTPases. Data are presented as means ± SEM. *$p < 0.05$, **$p < 0.01$, ***$p < 0.001$; ns, not significant.

to degrade FITC-gelatin matrix and invade a collagen layer in the Transwell chamber assay. PI4KIIβ-depleted MCF-7 cells degraded FITC-gelatin to an extent comparable to the highly invasive MDA-MDB-231 line (Figure 6, A and B). Furthermore, they displayed increased invasiveness and the ability to invade collagen ECM and cross the membrane toward a chemoattractant (Figure 6C). These findings indicate that PI4KIIβ suppresses cell invasion in vitro.

Loss of PI4KIIβ is associated with human cancers

A region of human chromosome 4 encompassing the gene for PI4KIIβ (PI4K2B) contains tumor suppressor genes associated with sporadic colorectal carcinoma (Zheng *et al.*, 2008). We therefore interrogated oncogenomic and transcriptomic data in the CBioPortal and Oncomine databases and found an association between heterozygous loss of PI4K2B and lung (squamous cell and adenocarcinoma), esophageal, pancreatic, prostate, breast, liver, and various other epithelial cancers (Figure 7A and Supplemental Figure S5). In pancreatic tumors, homozygous loss of PI4K2B was detected in 2.75% of samples, heterozygous loss in 43.1%, and gain in 12.8%. Copy number was normal in 39.44% (*n* = 109 samples; Figure 7B). In HCC, both PI4K2B alleles were deleted in 0.52%, 23.68% displayed heterozygous deletion, 64.73% had normal copy numbers, and 10.52% showed gain of PI4K2B (*n* = 190; Figure 7C). Significant reductions in PI4KIIβ mRNA expression were detected in invasive breast carcinoma (*n* = 59; Figure 7D). We also analyzed survival data in the small number of cases available (Ciriello *et al.*, 2015) and found that loss of PI4KIIβ expression correlated with poor survival in patients diagnosed with carcinoma of the breast (Figure 7E). Together these data support the hypothesis that loss of PI4KIIβ is a risk factor in cancers.

DISCUSSION

Here we identify a post-TGN trafficking pathway that negatively regulates endolysosomal traffic and the formation of invadopodia. Loss of the PI4KII isoforms had dramatically different and unexpected effects on the actin cytoskeleton. An additional and striking feature of PI4KIIβ-depleted cells was the appearance of mature and functional invadopodia on the ventral surface.

PI4KIIβ plays a role in the development of a migratory phenotype in HCC (Mazzocca *et al.*, 2008), but there is limited evidence for the direct involvement of mammalian PI4KII isozymes in actin regulation. In contrast, several studies have described PI4KII functions in post-TGN traffic through PI(4)P biosynthesis and direct binding to clathrin adaptors AP-1 and AP-3 (Wang *et al.*, 2003, 2007; Salazar *et al.*, 2005; Craige *et al.*, 2008), both pathways that contribute to endolysosomal traffic. PI4KIIα controls LE traffic of the EGFR (Minogue *et al.*, 2006), endolysosomal traffic mediated by AP-3 (Craige *et al.*, 2008), and that of lysosomal membrane proteins and hydrolases such as the enzyme β-glucocerebosidase (Jovic *et al.*, 2012). This explains the similar effects of PI4KIIα and PI4KIIβ depletion on EGFR degradation and LE traffic (Figure 4, I and J). PI4KIIβ localizes to the TGN and recruits AP-1, where it controls the endosomal sorting of Frizzled by traffic to degradative compartments (Wieffer *et al.*, 2013). There is therefore a substantial amount of data from our study and in published work indicating that each PI4KII contributes to TGN-EE/LE traffic by acting at different points in a pathway leading to lysosomal degradation. The other principal way in which the PI4KII isoforms differ is in the regulation of their PI4KII activity. The reported low activity of PI4KIIβ (Balla *et al.*, 2002) and the need to recruit this isoform to membranes (Jung *et al.*, 2011) illustrate the importance of regulating its activity and suggest that this isoform is subject to tight regulation.

Few studies have investigated the role of PI4KIIs in TGN PI(4)P synthesis. Our data demonstrate for the first time that the PI4KII enzymes synthesize separate TGN pools of PI(4)P that are defined by the markers syntaxin 6 and TGN46. This is consistent with our previous description of a

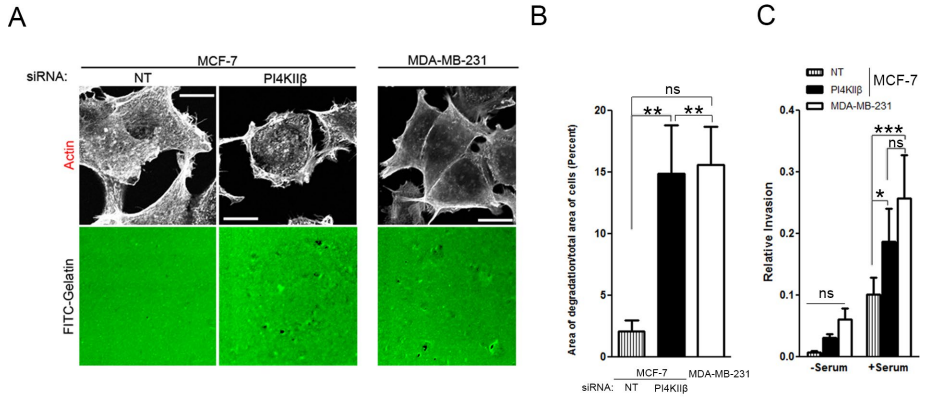

FIGURE 6: PI4KIIβ depletion is sufficient to confer a migratory and invasive phenotype. (A) siRNA-treated MCF-7 and untreated MDA-MB-231 cells were reseeded onto FITC-gelatin–coated coverslips (green) at 58 h posttransfection and then labeled for F-actin (red). (B) Percentage areas of proteolytic degradation per total cell in a 4×10^4 μm^2 field. Data are mean ± SEM (*n* = 30; experiments done in triplicate). (C) HeLa cells were reseeded onto collagen-coated Transwell inserts at 58 h posttransfection and placed in a chemoattractant (10% FCS) for 12 h. Histogram shows index of cell migration through an artificial barrier in response to chemoattractant. Data are mean ± SEM, *$p < 0.05$, **$p < 0.01$, ***$p < 0.001$; ns, not significant.

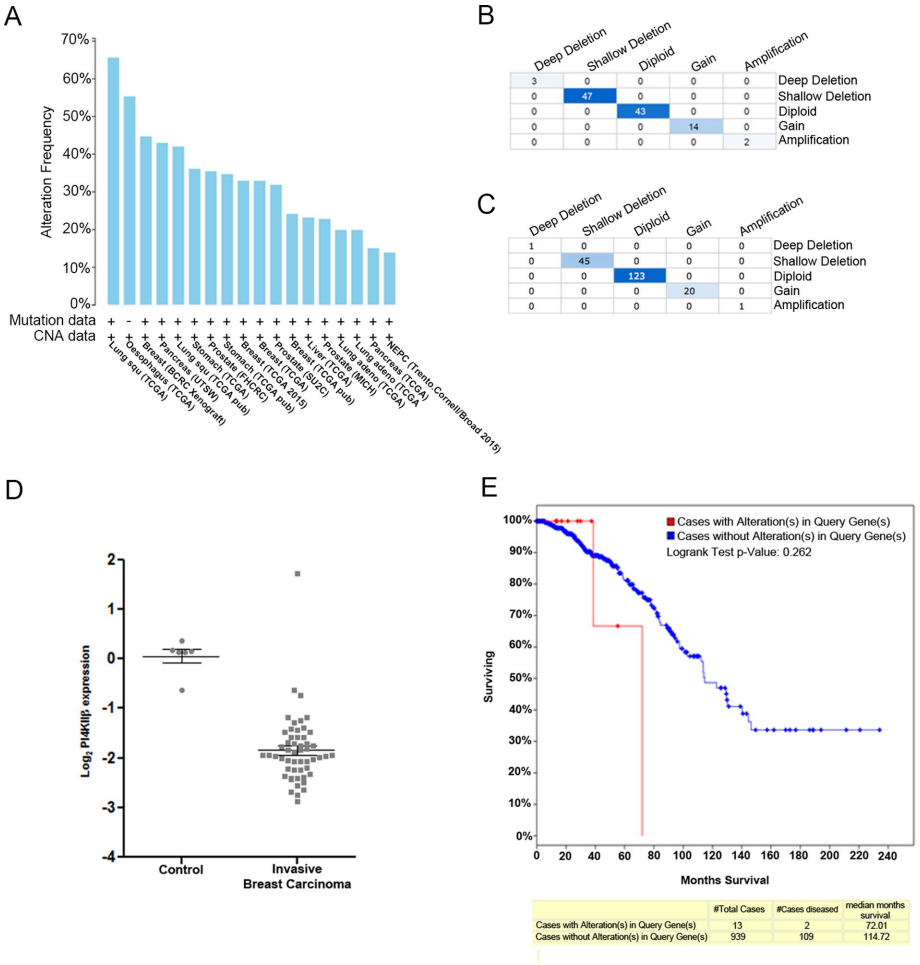

FIGURE 7: Database analysis shows that loss of PI4KIIβ expression is associated with cancers. (A) Cross-cancer copy number alteration (CNA) summary of 18 selected cancer studies (including lung, esophageal, breast, prostate, and pancreatic tumors) for heterozygous loss of the PI4K2B allele. Threshold: minimum 5% altered samples, cBioPortal analysis (Cerami *et al.*, 2012; Gao *et al.*, 2013). adeno, adenocarcinoma; NEPC, neuroendocrine prostate cancer; Squ, squamous cell carcinoma. Sources of the data are given in parentheses: TCGA, The Cancer Genome Atlas; BCRC, British Columbia Cancer Research Center; UTSW, University of Texas Southwestern; FHCRC, Fred Hutchinson Cancer Research Center; SU2C, Stand Up To Cancer/Prostate Cancer Foundation (PCF); MICH, University of Michigan. (B) PI4K2B putative copy number alterations for pancreatic cancers (deletion or amplification) was analyzed using cBioPortal. (C) Overall change in PI4K2B copy number (deletion or amplification) in HCC was analyzed using cBioPortal. (D) Analysis of PI4KIIβ mRNA expression (Oncomine) in recurrent breast carcinoma (Finak breast, reporter: A_23_P18598). (E) Overall Kaplan–Meier survival graph of breast carcinoma case analysis (cBioPortal) with PI4KIIβ expression alteration (Ciriello *et al.*, 2015).

TGN-endosomal compartment enriched in syntaxin 6 containing highly active PI4KIIα (Simonsen *et al.*, 1999; Waugh *et al.*, 2003). The structurally unrelated, wortmannin-sensitive PI4KIIIβ also contributes to PI(4)P synthesis in the Golgi of MDCK cells (Weixel *et al.*, 2005), indicating that the Golgi complex contains at least three metabolically separate PI(4)P pools.

Cells such as HeLa and MCF-7 normally display minimal invasive potential and typically have low levels of surface MT1-MMP, reflecting the importance of controlling surface metalloproteinase activity (Poincloux *et al.*, 2009). Loss of either PI4KII isoform led to increased levels of the metalloproteinase, consistent with a general impairment of endolysosomal degradative traffic; however, only depletion of PI4KIIβ caused increased levels of surface MT1-MMP, indicating that intracellular traffic of MT1-MMP was affected in an isoform-specific manner.

The reduced colocalization of MT1-MMP with Rab7, which acts at the EE-LE boundary, in both PI4KII-depleted cells demonstrates that the proteinase is not sorted to the LE. This is consistent with the elevated levels of MT1-MMP observed in both PI4KII knockdowns (Supplemental Figure S4C), the impaired degradation of the EGFR (Figure 4, I and J), and the failure of MT1-MMP to traffic to CD63-containing lysosomes (Supplemental Figure 4, A and B). The most dramatic change in colocalization was a PI4KIIβ-specific increase in association with Rab8 membranes. Rab8 operates in a post-Golgi exocytic pathway that determines directional traffic to protrusions of the plasma membrane (Hattula *et al.*, 2006) and is known to mediate the trafficking of MT1-MMP (Bravo-Cordero *et al.*, 2007). A mechanistic investigation of Rab8 was outside the scope of our study, but it is interesting to note that this GTPase was recently shown to regulate the cortical actin cytoskeleton (Bravo-Cordero *et al.*, 2016), suggesting that the mistrafficking of Rab8 may contribute to the actin phenotype.

We were unable to detect increased trafficking of MT1-MMP-GFP to invasive structures in live cell experiments; however, our attempts were fraught with technical difficulties arising from the substantial MT1-MMP signal present in multiple subcellular compartments that obscured invadopodia dynamics. The trafficking of MT1-MMP is known to be complex, and surface levels are controlled by endocytosis and exocytosis from several compartments (Poincloux *et al.*, 2009). The increased localization of MT1-MMP to the plasma membrane, increased association with invasive protrusions, loss of colocalization in Rab5- and Rab7-positive compartments, and increased colocalization with exocytic Rab8 membranes indicate that loss of PI4KIIβ and the associated pool of TGN PI(4)P causes disequilibrium between the endolysosomal and exocytic trafficking routes controlling plasma membrane levels of MT1-MMP. Our data support a model in which MT1-MMP traffic is directed away from the default endolysosomal pathway and forced into an exocytic pathway. One possible consequence of reduced MT1-MMP traffic into the endolysosomal pathway is increased recycling. Although we did not directly address this possibility, it remains likely because we also detected increased invadopodial localization of β1-integrin, a molecule known to be recycled through a pathway involving Rab8 and cotrafficked with MT1-MMP (Macpherson *et al.*, 2014). Of interest, the recent finding that PI4KIIα directs exocytic traffic of β1-integrin from endosomes to the plasma membrane when endosomal PI(3)P is lost (Ketel *et al.*, 2016) suggests that endosomal PI(4)$P^{PI4KII\alpha}$ may play a role in β1-integrin delivery. Further investigation is required to determine whether loss of PI(4)$P^{PI4KII\beta}$ results in an increase in PI(4)$P^{PI4KII\alpha}$ and whether this is accompanied by increased β1-integrin recycling.

Integrin traffic to the plasma membrane plays important roles in tissue organization and is known to be dependent on PI(3)P (Ribeiro *et al.*, 2011). Cross-talk between this PI monophosphate and the PI(4)P produced by the PI4KIIs is an unanswered question.

The conversion of the minimally invasive HeLa and MCF-7 cell lines to an invasive phenotype and the fact that tumor suppressor genes map closely to the chromosomal location of the PI4K2B allele (Zheng *et al.*, 2008) led us to perform database searches. These showed that loss of heterozygosity of the PI4K2B allele and PI4KIIβ underexpression were associated with numerous cancers of epithelial origin. PI4KIIβ underexpression was also associated with poorer patient survival; however, the low statistical power of the studies led to a relatively low probability value ($p = 0.262$). Although we are cautious in drawing conclusions, we are aware that this finding may be highly significant and therefore speculate that PI4KIIβ acts as a metastasis suppressor by maintaining PI(4)P-dependent post-TGN traffic into the endolysosomal pathway. The association of PI4KIIβ with relatively common human cancers (lung, breast, liver, pancreas, and others) warrants further investigation, particularly because of the possibility that this putative suppressor pathway could be rescued by inhibition of PI(4)P phosphatases acting at the TGN.

It is notable that a developmental role for PI4KIIβ in zebrafish has been described (Wieffer *et al.*, 2013). The pathological process of tumor cell invasion has many similarities with important processes during embryogenesis along with neurite outgrowth and angiogenesis. It is therefore possible that PI4KIIβ activity is subject to regulation controlling physiological invasion. This hypothesis points to a PI(4)P-regulated switch that determines the decision between lysosomal degradation of cargoes and their traffic to the plasma membrane that may be fundamentally important in the intracellular traffic of key molecules such as integrins and matrix metalloproteinases that determine tissue remodeling during development.

MATERIALS AND METHODS

Cell lines, culture, and transfection

HeLa and MCF7 cell lines were cultured in DMEM (Life Technologies, Paisley, UK) supplemented with 10% fetal bovine serum (FBS; Sigma-Aldrich, Dorset, UK) and maintained at 37°C and 5% CO_2. MDA-MB-231 cells were cultured in Leibowitz's L-15 medium (Life Technologies) supplemented with 15% FBS and 2 mM L-glutamine (Life Technologies) and maintained at 37°C, 0.1% CO_2. All media were supplemented with antibiotics (1000 U/ml penicillin and 0.1 mg/ml streptomycin; Sigma-Aldrich). DharmaFECT (GE Healthcare Dharmacon, Lafayette, CO) and Lipofectamine (Life Technologies) were used to transfect siRNAs and plasmids, respectively.

Antibodies and reagents

All primary antibodies with corresponding dilutions are listed in Supplemental Table S1. Highly cross-adsorbed Alexa Fluor–conjugated secondary antibodies and Alexa Fluor–conjugated phalloidin (1:250 dilution) were purchased from Molecular Probes (Life Technologies). Hoechst 33342 trihydrochloride was also from Molecular Probes and was used at 1:5000 for nuclear staining. Human recombinant EGF was purchased from Sigma-Aldrich. Unless otherwise stated, other reagents were from Sigma Aldrich.

Plasmids

siRNA-resistant GFP-tagged PI4KIIα and hemagglutinin-tagged PI4KIIβ were generous gifts from Volker Haucke (Leibniz Institut für Molekulare Pharmakologie, Berlin, Germany). mCherry and GFP-tagged CI-M6PR were kindly provided by Mihaela Anitei (Technische Universität, Dresden, Germany).

Small interfering RNAs

We silenced PI4KIIα and PI4KIIβ using ON-TARGET*plus* SMARTpools siRNA oligonucleotides (GE Healthcare Dharmacon). Each comprised a mix of four siRNA duplexes targeting specific sequences within the named genes. We also used an ON-TARGET*plus* nontargeting pool (D-001810-10-05) as control. Gene silencing was confirmed by Western blotting of whole-cell lysates. PI4KII-knockdown phenotypes were rescued using single siRNA duplexes and the ectopic expression of siRNA resistant plasmids as described previously (Mossinger *et al.*, 2012; Wieffer *et al.*, 2013). Further details are given in the Supplemental Materials and Supplemental Table S2.

Western immunoblotting

Cells were lysed in RIPA buffer (50 mM Tris-HCl, pH 7.6, 150 mM NaCl, 0.5% sodium deoxycholate, 1% Triton X-100, 10% glycerol, 0.5 mM ethylene diamine tetraacetic acid [EDTA], 0.5 mM ethylene glycol-bis(β-aminoethyl ether)-*N*,*N*,*N*′,*N*′-tetraacetic acid [EGTA], 10 mM sodium fluoride, 10 mM sodium pyrophosphate, 0.2 mM Na_3VO_4) and 1× cOmplete Protease Inhibitor (Roche, Mannheim, Germany). Protein content was determined using the Lowry method (Bio-Rad, Hertfordshire, UK), and lysates were solubilized in 2× Laemmli sample buffer, separated using SDS–PAGE, blotted, and probed with respective antibodies. Blots were imaged on a FluorChem M Multifluor imaging system (ProteinSimple, San Jose, CA) and analyzed by densitometry using its gel analysis function.

Immunofluorescence microscopy

Cells were grown on glass coverslips, fixed, and probed with antibodies of interest as previously (Minogue *et al.*, 2006). Unless otherwise stated, images were acquired using the 63×/1.4 numerical aperture lens on a Zeiss LSM 510 confocal microscope. Randomly chosen representative fields were selected and 12-bit images acquired using identical detector gain and offset settings. Images were quantitatively analyzed for fluorescence intensities, pixel correlations, area measurements, and cell densities using ImageJ software (National Institutes of Health, Bethesda, MD). Full details are available in the Supplemental Materials.

Fluorescent matrix degradation

The ability of cells to degrade the extracellular matrix was analyzed using fluorescent gelatin matrix–coated culture dishes prepared according to Bowden *et al.* (1999). Targeted or control siRNA-transfected cells were seeded onto FITC-gelatin–coated coverslips and cultured for 12–18 h. Matrix degradation was calculated as the total area of matrix degradation (black holes) per total cell area expressed as a percentage (full details are given in the Supplemental Materials).

MT1-MMP trafficking

We used an established method (Kean *et al.*, 2009). Briefly, MCF-7 cells were reseeded onto coverslips thinly coated with collagen (5 μg/cm^2) at 36 h posttransfection and grown in complete DMEM for 20 h at 37°C. Cells were then serum starved for 4 h to facilitate internalization of MT1-MMP. For trafficking of endogenous MT1-MMP, cells were pulsed with anti–MT1-MMP antibody (Abcam, Cambridge, UK) for 1 h at 4°C. Cells were subsequently fixed with 3.7% formaldehyde, permeabilized, and immunostained.

For flow cytometry experiments, we induced internalization of MT1-MMP by serum starvation and stimulated surface expression as described. Cells were lifted using FACS buffer (5 mM EDTA in phosphate-buffered saline [PBS], pH 7.4) and subsequent steps carried out at 4°C. Cells were probed with rabbit anti–MT1-MMP (Abcam)

for 1 h, washed three times with PBS, and then labeled with anti–rabbit Alexa Fluor antibody. Cells were analyzed using a FACS LSRII cell sorter (BD Biosciences, Oxford, UK), and ~10,000 cells were counted per sample. Postacquisition analysis was performed using Flowjo software, version V10 (FlowJo LLC, Ashland, OR).

Transwell migration assay

This was performed in 8-μm-pore, collagen-coated Transwell chambers (Corning, Tewksbury, MA). Cells were transfected with target or control siRNA in six-well plates and, after 48 h, resuspended in serum-free medium and seeded at 5×10^4 into the upper chamber of the Transwell. Cells were allowed to migrate toward 10% FBS plus DMEM for 12 h. Migratory cells at the lower chamber were fixed and stained with Alexa 488–conjugated phalloidin, imaged using similar optical settings (20× Objective, Zeiss LSM 510 confocal microscope), and counted in five random fields using ImageJ. Histograms represent relative invasion of the Transwell chamber, calculated as the number of cells counted at the lower chamber relative to the total number of cells seeded onto the upper chamber (details are give in the Supplemental Materials).

Data analysis

Prism 5 (GraphPad, La Jolla, CA) was used for statistical analysis. Data are presented as mean ± SEM from at least three independent experiments. Statistical comparisons were performed using one-way analysis of variance followed by Tukey's posttest at a 95% confidence interval.

Oncogenomic database analysis

The cBIO Cancer Genomics Portal (http://cbioportal.org/; Cerami *et al.*, 2012; Gao *et al.*, 2013) and Oncomine (Rhodes *et al.*, 2004) are open access resources for cancer genomics data sets containing data from 69 cancer genomics studies with 17,177 samples (cBIO) and 715 data sets with 86,733 samples (Oncomine). Heterozygous loss of the PI4K2B allele was analyzed in all cancers, as were copy number alterations in pancreatic cancers and hepatocellular carcinoma. In addition, correlations of PI4KIIβ mRNA expression, recurrence, metastatic events, or overall survival in breast cancer cases were investigated.

ACKNOWLEDGMENTS

We are grateful to Volker Haucke (Leibniz Institut für Molekulare Pharmakologie, Berlin, Germany) for reagents. GFP-CI-M6PR was provided by Mihaela Anitei (Technische Universität, Dresden, Germany). We acknowledge Justin Hsuan, in whose laboratory the studies were initiated. We are grateful to Robin Ketteler (Laboratory for Molecular Cell Biology, University College London) for help and advice. This work was supported by a National Universities Commission (NUC) of Nigeria PRESSID Scholarship (G.O.A. and S.M.) and Medical Research Council core funding to J.K. (ref. MC_EX_G0800785).

REFERENCES

Balla A, Balla T (2006). Phosphatidylinositol 4-kinases: old enzymes with emerging functions. Trends Cell Biol 16, 351–361.

Balla A, Tuymetova G, Barshishat M, Geiszt M, Balla T (2002). Characterization of type II phosphatidylinositol 4-kinase isoforms reveals association of the enzymes with endosomal vesicular compartments. J Biol Chem 277, 20041–20050.

Bowden ET, Barth M, Thomas D, Glazer RI, Mueller SC (1999). An invasion-related complex of cortactin, paxillin and PKCmu associates with invadopodia at sites of extracellular matrix degradation. Oncogene 18, 4440–4449.

Bravo-Cordero JJ, Cordani M, Soriano SF, Diez B, Munoz-Agudo C, Casanova-Acebes M, Boullosa C, Guadamillas MC, Ezkurdia I, Gonzalez-Pisano D, *et al.* (2016). A novel high-content analysis tool reveals Rab8-driven cytoskeletal reorganization through Rho GTPases, calpain and MT1-MMP. J Cell Sci 129, 1734–1749.

Bravo-Cordero JJ, Marrero-Diaz R, Megias D, Genis L, Garcia-Grande A, Garcia MA, Arroyo AG, Montoya MC (2007). MT1-MMP proinvasive activity is regulated by a novel Rab8-dependent exocytic pathway. EMBO J 26, 1499–1510.

Cerami E, Gao J, Dogrusoz U, Gross BE, Sumer SO, Aksoy BA, Jacobsen A, Byrne CJ, Heuer ML, Larsson E, *et al.* (2012). The cBio cancer genomics portal: an open platform for exploring multidimensional cancer genomics data. Cancer Discov 2, 401–404.

Ciriello G, Gatza ML, Beck AH, Wilkerson MD, Rhie SK, Pastore A, Zhang H, McLellan M, Yau C, Kandoth C, *et al.* (2015). Comprehensive molecular portraits of invasive lobular breast cancer. Cell 163, 506–519.

Craige B, Salazar G, Faundez V (2008). Phosphatidylinositol-4-kinase type II alpha contains an AP-3-sorting motif and a kinase domain that are both required for endosome traffic. Mol Biol Cell 19, 1415–1426.

Destaing O, Planus E, Bouvard D, Oddou C, Badowski C, Bossy V, Raducanu A, Fourcade B, Albiges-Rizo C, Block MR (2010). beta1A integrin is a master regulator of invadosome organization and function. Mol Biol Cell 21, 4108–4119.

Egeblad M, Werb Z (2002). New functions for the matrix metalloproteinases in cancer progression. Nat Rev Cancer 2, 161–174.

Gao J, Aksoy BA, Dogrusoz U, Dresdner G, Gross B, Sumer SO, Sun Y, Jacobsen A, Sinha R, Larsson E, *et al.* (2013). Integrative analysis of complex cancer genomics and clinical profiles using the cBioPortal. Sci Signal 6, pl1.

Garcia E, Machesky LM, Jones GE, Anton IM (2014). WIP is necessary for matrix invasion by breast cancer cells. Eur J Cell Biol 93, 413–423.

Hammond GR, Machner MP, Balla T (2014). A novel probe for phosphatidylinositol 4-phosphate reveals multiple pools beyond the Golgi. J Cell Biol 205, 113–126.

Hattula K, Furuhjelm J, Tikkanen J, Tanhuanpaa K, Laakkonen P, Peranen J (2006). Characterization of the Rab8-specific membrane traffic route linked to protrusion formation. J Cell Sci 119, 4866–4877.

Henmi Y, Morikawa Y, Oe N, Ikeda N, Fujita A, Takei K, Minogue S, Tanabe K (2016). PtdIns4KIIalpha generates endosomal PtdIns(4)P and is required for receptor sorting at early endosomes. Mol Biol Cell 27, 990–1001.

Hotary K, Li XY, Allen E, Stevens SL, Weiss SJ (2006). A cancer cell metalloprotease triad regulates the basement membrane transmigration program. Genes Dev 20, 2673–2686.

Jovic M, Kean MJ, Szentpetery Z, Polevoy G, Gingras AC, Brill JA, Balla T (2012). Two phosphatidylinositol 4-kinases control lysosomal delivery of the Gaucher disease enzyme, beta-glucocerebrosidase. Mol Biol Cell 23, 1533–1545.

Jung G, Barylko B, Lu D, Shu H, Yin H, Albanesi JP (2011). Stabilization of phosphatidylinositol 4-kinase type IIbeta by interaction with Hsp90. J Biol Chem 286, 12775–12784.

Kean MJ, Williams KC, Skalski M, Myers D, Burtnik A, Foster D, Coppolino MG (2009). VAMP3, syntaxin-13 and SNAP23 are involved in secretion of matrix metalloproteinases, degradation of the extracellular matrix and cell invasion. J Cell Sci 122, 4089–4098.

Ketel K, Krauss M, Nicot AS, Puchkov D, Wieffer M, Muller R, Subramanian D, Schultz C, Laporte J, Haucke V (2016). A phosphoinositide conversion mechanism for exit from endosomes. Nature 529, 408–412.

Li J, Lu Y, Zhang J, Kang H, Qin Z, Chen C (2010). PI4KIIalpha is a novel regulator of tumor growth by its action on angiogenesis and HIF-1alpha regulation. Oncogene 29, 2550–2559.

Li J, Zhang L, Gao Z, Kang H, Rong G, Zhang X, Chen C (2014). Dual inhibition of EGFR at protein and activity level via combinatorial blocking of PI4KIIalpha as anti-tumor strategy. Protein Cell 5, 457–468.

Luo X, Wasilko DJ, Liu Y, Sun J, Wu X, Luo ZQ, Mao Y (2015). Structure of the Legionella virulence factor, SidC reveals a unique PI(4)P-specific binding domain essential for its targeting to the bacterial phagosome. PLoS Pathog 11, e1004965.

Macpherson IR, Rainero E, Mitchell LE, van den Berghe PV, Speirs C, Dozynkiewicz MA, Chaudhary S, Kalna G, Edwards J, Timpson P, Norman JC (2014). CLIC3 controls recycling of late endosomal MT1-MMP and dictates invasion and metastasis in breast cancer. J Cell Sci 127, 3893–3901.

Mazzocca A, Liotta F, Carloni V (2008). Tetraspanin CD81-regulated cell motility plays a critical role in intrahepatic metastasis of hepatocellular carcinoma. Gastroenterology 135, 244–256.e241.

Minogue S, Waugh MG (2012). The phosphatidylinositol 4-kinases: don't call it a comeback. Subcell Biochem 58, 1–24.

Minogue S, Waugh MG, De Matteis MA, Stephens DJ, Berditchevski F, Hsuan JJ (2006). Phosphatidylinositol 4-kinase is required for endosomal trafficking and degradation of the EGF receptor. J Cell Sci 119, 571–581.

Mossinger J, Wieffer M, Krause E, Freund C, Gerth F, Krauss M, Haucke V (2012). Phosphatidylinositol 4-kinase IIalpha function at endosomes is regulated by the ubiquitin ligase Itch. EMBO Rep 13, 1087–1094.

Paz H, Pathak N, Yang J (2014). Invading one step at a time: the role of invadopodia in tumor metastasis. Oncogene 33, 4193–4202.

Poincloux R, Lizarraga F, Chavrier P (2009). Matrix invasion by tumour cells: a focus on MT1-MMP trafficking to invadopodia. J Cell Science 122, 3015–3024.

Rhodes DR, Yu J, Shanker K, Deshpande N, Varambally R, Ghosh D, Barrette T, Pandey A, Chinnaiyan AM (2004). ONCOMINE: a cancer microarray database and integrated data-mining platform. Neoplasia 6, 1–6.

Ribeiro I, Yuan L, Tanentzapf G, Dowling JJ, Kiger A (2011). Phosphoinositide regulation of integrin trafficking required for muscle attachment and maintenance. PLoS Genet 7, e1001295.

Sabeh F, Ota I, Holmbeck K, Birkedal-Hansen H, Soloway P, Balbin M, Lopez-Otin C, Shapiro S, Inada M, Krane S, *et al*. (2004). Tumor cell traffic through the extracellular matrix is controlled by the membrane-anchored collagenase MT1-MMP. J Cell Biol 167, 769–781.

Salazar G, Craige B, Wainer BH, Guo J, De Camilli P, Faundez V (2005). Phosphatidylinositol-4-kinase type II alpha is a component of adaptor protein-3-derived vesicles. Mol Biol Cell 16, 3692–3704.

Simonsen A, Gaullier JM, D'Arrigo A, Stenmark H (1999). The Rab5 effector EEA1 interacts directly with syntaxin-6. J Biol Chem 274, 28857–28860.

Steffen A, Le Dez G, Poincloux R, Recchi C, Nassoy P, Rottner K, Galli T, Chavrier P (2008). MT1-MMP-dependent invasion is regulated by TI-VAMP/VAMP7. Curr Biol 18, 926–931.

Tatin F, Varon C, Genot E, Moreau V (2006). A signalling cascade involving PKC, Src and Cdc42 regulates podosome assembly in cultured endothelial cells in response to phorbol ester. J Cell Sci 119, 769–781.

Taunton J, Rowning BA, Coughlin ML, Wu M, Moon RT, Mitchison TJ, Larabell CA (2000). Actin-dependent propulsion of endosomes and lysosomes by recruitment of N-WASP. J Cell Biol 148, 519–530.

Wang J, Sun HQ, Macia E, Kirchhausen T, Watson H, Bonifacino JS, Yin HL (2007). PI4P promotes the recruitment of the GGA adaptor proteins to the trans-Golgi network and regulates their recognition of the ubiquitin sorting signal. Mol Biol Cell 18, 2646–2655.

Wang YJ, Wang J, Sun HQ, Martinez M, Sun YX, Macia E, Kirchhausen T, Albanesi JP, Roth MG, Yin HL (2003). Phosphatidylinositol 4 phosphate regulates targeting of clathrin adaptor AP-1 complexes to the Golgi. Cell 114, 299–310.

Waugh MG, Minogue S, Anderson JS, Balinger A, Blumenkrantz D, Calnan DP, Cramer R, Hsuan JJ (2003). Localization of a highly active pool of type II phosphatidylinositol 4-kinase in a p97/valosin-containing-protein-rich fraction of the endoplasmic reticulum. Biochem J 373, 57–63.

Weixel KM, Blumental-Perry A, Watkins SC, Aridor M, Weisz OA (2005). Distinct Golgi populations of phosphatidylinositol 4-phosphate regulated by phosphatidylinositol 4-kinases. J Biol Chem 280, 10501–10508.

Wieffer M, Cibrian Uhalte E, Posor Y, Otten C, Branz K, Schutz I, Mossinger J, Schu P, Abdelilah-Seyfried S, Krauss M, Haucke V (2013). PI4K2beta/AP-1-based TGN-endosomal sorting regulates Wnt signaling. Curr Biol 23, 2185–2190.

Wiesner C, El Azzouzi K, Linder S (2013). A specific subset of RabGTPases controls cell surface exposure of MT1-MMP, extracellular matrix degradation and three-dimensional invasion of macrophages. J Cell Sci 126, 2820–2833.

Williams KC, Coppolino MG (2011). Phosphorylation of membrane type 1-matrix metalloproteinase (MT1-MMP) and its vesicle-associated membrane protein 7 (VAMP7)-dependent trafficking facilitate cell invasion and migration. J Biol Chem 286, 43405–43416.

Yu X, Zech T, McDonald L, Gonzalez EG, Li A, Macpherson I, Schwarz JP, Spence H, Futo K, Timpson P, *et al*. (2012). N-WASP coordinates the delivery and F-actin-mediated capture of MT1-MMP at invasive pseudopods. J Cell Biol 199, 527–544.

Zheng HT, Jiang LX, Lv ZC, Li DP, Zhou CZ, Gao JJ, He L, Peng ZH (2008). Are there tumor suppressor genes on chromosome 4p in sporadic colorectal carcinoma? World J Gastroenterol 14, 90–94.

Supplemental Materials

Molecular Biology of the Cell

Alli-Balogun et al.

Supplemental Materials

Phosphatidylinositol 4-kinase IIβnegatively regulates invadopodiaformation and suppresses an invasive cellular phenotype.

GaniyuOlabanjiAlli-Balogun, Christina A. Gewinner, Ruth Jacobs, Janos Kriston-Vizi, Mark G. Waugh and Shane Minogue.

Antibodies

Mouse monoclonal anti-PI4KIIα has been described (Simons *et al.*, 2009) and polyclonal anti-PI4KIIβ(HPA004099)was from Atlas Antibodies (Sigma-Aldrich, St. Louis, MO). Mouse monoclonal anti γ-adaptin(AP-1, A4200) was from Sigma-Aldrich. Rabbit monoclonal anti-GAPDH (14C10) and anti-EGFR (D38B1) were from Cell Signalling Technology (CST, New England BioLabs, Hertfordshire, UK) as were antibodies to cortactin (H222), EEA1 (C45B10), Glutathione-S-transferase (GST, (26H1)),phospho-Tyrosine (P-Tyr-100), Rab5 (C8B1), Rab7 (D95F2), Rab8 (D22D8), Rab9 (D52G8), Rab11 (D4F5), syntaxin6 (C34B2). Horseradish-peroxidase (HRP)-linked secondary antibodies were also from Cell Signalling Technology. Antibodies to α-tubulin and highly crossed-adsorbed Alexa Fluor® conjugated secondary antibodies were from Molecular probes (Life Technologies, Ltd, Paisley, UK). Antibodies to β1-integrin (CD29 (Clone 18/CD29)), and CD63 were from BD. Anti-TGN46 antibody was purchased from AbDSerotec (BioRad Labs, Inc). Anti MT1-MMP antibodies (ab78738 and ab3644) were from Abcam while anti-MT1-MMP14 (LEM2/15.8) was purchased from Merck (Merck Millipore). Antibody dilutions are givenin Table S1.

Table S1. Antibodies and their respective dilutions for different applications

Antigen	Host Species	Isotype	Dilutions		
			Immuno-fluorescence	Western Blotting	Flow cytometry
Anti-mouse IgG, Alexa Fluor® conjugates	Goat	Polyclonal	1:500		1:500
Anti-rabbit IgG, Alexa Fluor® conjugates	Goat	Polyclonal	1:500		1:500
Anti-sheep IgG, Alexa Fluor® conjugates	Donkey	Polyclonal	1:500		
CD63	Mouse	Monoclonal	1:400		
Cortactin (H222)	Rabbit	Polyclonal	1:100	1:1000	
EEA1 (C45B10)	Rabbit	Monoclonal	1:100		
EGF Receptor(D38B1)	Rabbit	Monoclonal		1:1000	
GAPDH (14C10)	Rabbit	Monoclonal		1:1000	
GST (26H1)	Mouse	Monoclonal	1:800		
HRP-Linked anti-mouseIgG	Horse	Polyclonal		1:1500	
HRP-Linked anti-rabbit IgG	Goat	Polyclonal		1:1500	
MT1-MMP ([LEM-2/15.8)]	Mouse	Monoclonal	10 µg/ml		
MT1-MMP ([LEM-2/63.1)]	Mouse	Monoclonal	1 µg/ml		
MT1-MMP (ab3644)	Rabbit	Polyclonal	1 µg/ml	1:500	1:50
Phospho-Tyrosine	Mouse	Monoclonal	1:1600	1:2000	
PI4KIIα	Mouse	Monoclonal	1:6	1:4	
PI4KIIβ	Rabbit	Polyclonal	1:32	1:250	
Rab11 (D4F5)	Rabbit	Monoclonal	1:100		
Rab5 (C8B1)	Rabbit	Monoclonal	1:200		

Rab7 (D95F2)	Rabbit	Monoclonal	1:100	
Rab8 (D22D8)	Rabbit	Monoclonal	1:200	
Rab9 (D52G8)	Rabbit	Monoclonal	1:100	
Syntaxin6 (C34B2)	Rabbit	Monoclonal	1:100	
TGN46	Sheep	Polyclonal	1:250	
α-Tubulin	Mouse	Monoclonal		1:2000
β1-Integrin (Clone 18/CD29)	Mouse	Monoclonal	1:100	
γ-Adaptin (AP-1)	Mouse	Monoclonal	1:200	

Supplemental Methods

Gene Silencing

ON-TARGET*plus*SMARTpool™siRNA oligonucleotides targeting PI4K2A or PI4K2B comprised a mix of four siRNA duplexes targeting specific sequences within the named genes (Table S2) - were purchased from Dharmacon™(GE Healthcare). Cells were at approximately 30% confluency on the day of transfection. Transfection mix containing Oligos and DharmaFECT4 transfection reagent was prepared according to the manufacturer's protocol, applied for 4-6 hours followed by replacement with complete medium. Unless otherwise stated, cells were cultured for 72 hours prior to analysis. For rescue experiments, the following siRNAs were used; PI4KIIα: GGAUCAUUGCUGUCUUCAAUU (Mössinger *et al.*, 2012), PI4KIIβ: GGUUCAAGUGGAAGUUACUUU(Wieffer *et al.*, 2013) (Dharmacon).siRNA silencing was repeated after 48 hours with or without the addition of siRNA resistant plasmids to the transfection mix using the Lipofectamine2000 protocol (Invitrogen). At 4 hours post transfection, medium was replaced with complete medium and cells were cultured for 24 hours prior to analysis.

EGFR degradation assay

At 54 hours post-transfection, siRNA treated cells were serum starved in 0.5% FBS (in DMEM) for 18 hours. This was followed by two rinses in PBS and treatment with10µg/ml cycloheximide for one hour to inhibit nascent synthesis of receptor. Following two rinses with PBS, cells were treated with 100ng/ml EGF ligand for indicated times (Figure 4I) and then lysed in RIPA buffer. Protein content was quantified using the DC protein assay reagent (Bio-Rad), lysates resolved by SDS-PAGE and analysed by western blotting.

Table S2:ON-TARGET*plus*SMARTpool targeting 4 different sequences within the primary transcripts of target genes.

Target gene	siRNA sequence (5'-3')	Target Region in primary transcript
PI4K2A	GGUUGGUGGUGCUGGAUUA	944-962
	CAACACUGAUCGAGGCAAU	972-990
	GAGACGAGCCCACUAGUGU	64-82
	GCAUCGGGCUACCACCAAA	806-824
PI4K2B	GGUAGUAAAUGUCAGAGUA	1575-1593
	GUUACAAGGAGGCUGAAUA	918-936
	UCUCAAGGUUCAAGUGGAA	512-530
	UGGUUUGGCUUGUCAGUGA	759-777

Membrane lipid staining

HeLa cells on 13mm glass coverslips were treated with 10µM wortmannin for 30 minutes (Balla *et al.*, 1997) followed by two rinses in PBS. Then we employed a previously described method (Hammond *et al.*, 2009) to preserve Golgi membranes. In details, cells were fixed with 2% formalin(v/v in PBS) for 15 minutes at room

temperature. Following two rinses in PBS+50mM, cells were permeabilised by incubating with 20μM digitonin in buffer A (20mM PIPES (pH6.8), NH_4Cl, 137 mMNaCl, 2.7 mMKCl) for 5 minutes at room temperature. Coverslips were rinsed thrice with buffer A to remove digitonin and then cells were blocked with buffer A supplemented with 1% BSA and 50mM NH_4Cl. 0.5 μg/ml GST-P4C (Echelon Biosciences, PI(4)P grip) was also included in the blocking buffer as a reporter for PI(4)P. Following incubation for 45 minutes at room temperature, GST-tagged proteins were removed by three washes with buffer A. We then probed with antibodies as previously described.

Preparation of gelatin coated dishes/culture plates

To coat each well of a 6-well plate with gelatin(Sigma-Aldrich), 2ml 0.2% gelatin (w/v in PBS) was applied to each well and incubated for 10 minutes at 4^{o}C on a rocking platform to allow solidification. Excess gelatin was aspirated and then 2ml 0.5% glutaraldehyde (v/v, in PBS) was pipetted into each well of a 6-well plate followed by incubation for 30 minutes at 4^{o}C with gentle rocking. Each well was subsequently washed three times with PBS followed by equilibration with culture medium at 37^{o}C for 30 minutes.

Preparation of fluorescent labelled coverslips

We used a previously described method (Bowden *et al.*, 2001). In details, approximately 200μl FITC-conjugated gelatinwas pipetted onto clean 13 mm glass coverslips in 24-well plates and then incubated on ice for 30 minutes. Excess FITC-gelatinwas gently aspirated and coated coverslips were treated with 0.5% glutaraldehyde (v/v in PBS) for 15 minutes at 4^{o}C. Coverslips were washed thrice (5 minute per wash) with PBS and then treated with 0.5% sodium borohydride (v/v in PBS) for 3 minutes at room temperature to quench glutaraldehyde auto-fluorescence. Coverslips were washed three timeswith PBS and then equilibrated with serum free medium for 30 minutes prior to cell seeding.

Preparation of collagen coated coverslips

To prepare thin layers of collagen matrices on glass coverslips, 50μg/mL of type I collagen(Gibco®) was prepared in 20mM acetic acid as described by the manufacturer

and then added at 5µg/cm^2 to each cover slip (100 µl required to coat a 13 mm coverslip). Coated coverslips were incubated at room temperature for one hour. Excess solution was carefully aspirated from each well followed by three rinses with sterile 1x PBS to remove the acid, prior to cell seeding.

To prepare 3D-collagen (thick layer), type I collagen was neutralised on ice to 2 mg/ml as described by the manufacturer. 13 mm glass coverslips in 24-well plates were coated with 0.1 ml neutralised collagen and allowed to polymerise for 30 minutes at 37^{o}C in humidified incubator.

Image Analysis

Quantitation of fluorescent intensities

Fluorescent intensities were quantified (Hammond *et al.*, 2009) with some modifications with the aid of the NIH ImageJ software. Images were converted to greyscale and thresholded using the same parameters across all fields. Regions of interest were then selected using the ROI command and integrated pixel intensities were measured at randomly selected fields. The integrated pixel intensity, *I* was normalized to pooled results across independent experiments. This was done using the following relation;

$$Normalised\ integrated\ fluorescence = \frac{(I - Ibg)}{Ictrl - Ibg}$$

Where I_{ctrl}represents the mean intensity for the control siRNA transfected cells in this case and I_{bg}represents the intensity of the background specimen in which antibodies or lipid binding probes were omitted.

Colocalisation analysis

Multi-channel confocal image stacks were converted to 8-bit single images and pixel co-localisation in two different channels was analysed using the Pearson's correlation coefficient (r) with the aid of the JACoP plugin on ImageJ(Bolte and Cordelières, 2006).

Quantitative analysis of actin based structures

This was done using ImageJ v1.50f with Java version 1.6.0_37 (64 bit) running under Linux (kernel version 3.2.0-97-generic). Multi-channel, 8-bit, fluorescent images were segmented using global intensity thresholds (Thr) for (red) and (green)such that ThrG=25 on the actin channel and ThrR=73 on the anti-pY channel. We then computed the total area of actin and anti-pY foreground pixels on each images using the Measure command of ImageJ. The ratio of the segmented anti-pY/actin area was calculated using LibreOfficeCalc (version 5.0.4.2).

Relative invasion

Relative invasion of the Transwell migration chamber was calculated by dividing the number of cells that migrated to the lower chamber in response to chemoattractantby the number of cells seeded (5×10^4) onto the serum-free upper chamber.

$$Relative\ invasion = \left(\frac{Number\ of\ cells\ invaded}{5\times10^4}\right)$$

Analysis of matrix degradation

Confocal images of F-actin and degraded matrix were captured using a Nikon confocal microscope equipped with NIS-nd2 software. Experiments were carried out in triplicates with at least 20 cells captured per experiment. The ImageJ software was used to compute the area of degradation in a $4x10^4\mu m^2$ field and the number of cells for each field. The total degraded area was expressed as a percentage of the total cell area.

Supplemental Figure Legends

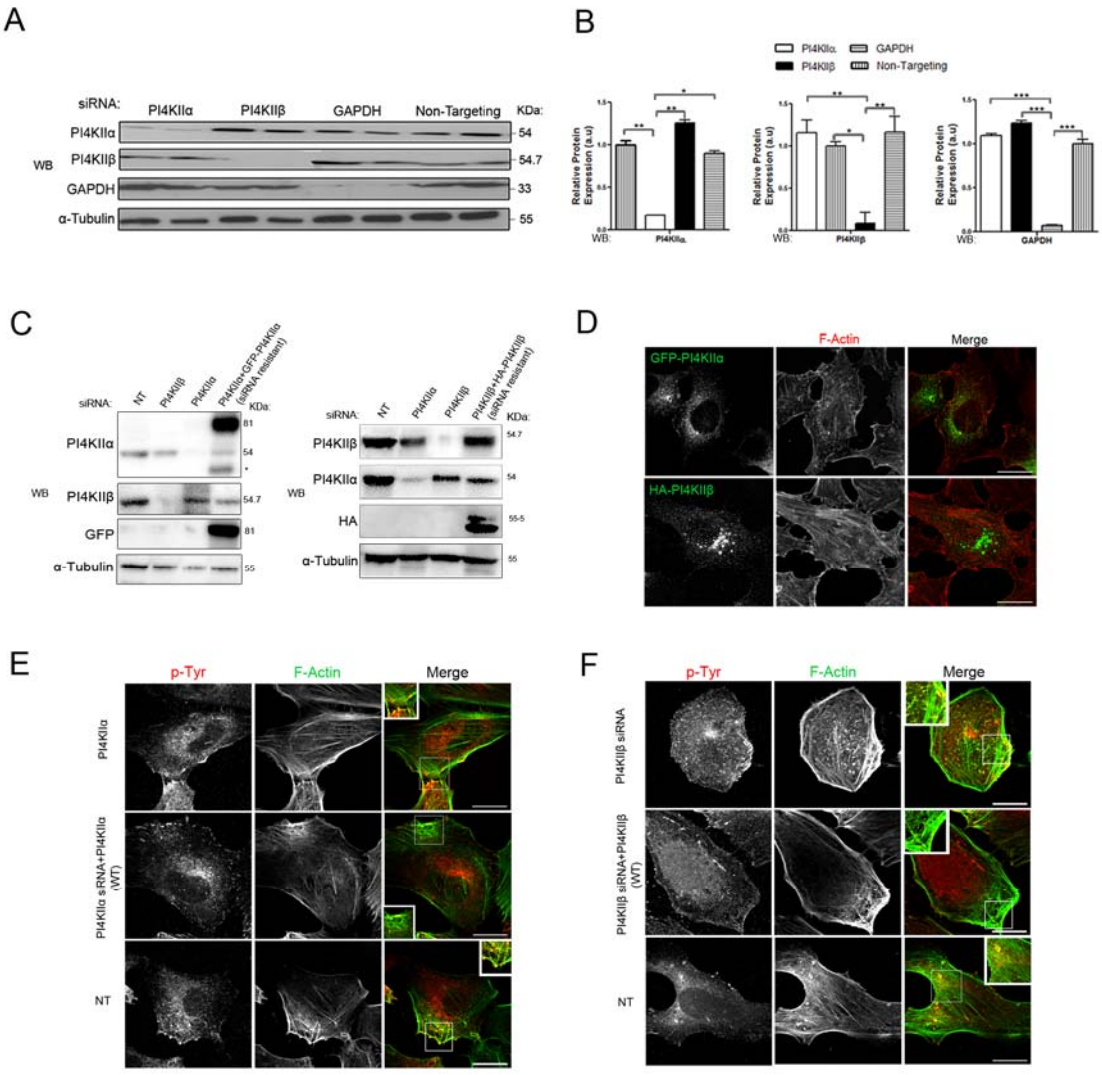

ALLI-BALOGUN, et al_SUPPLEMENTAL FIGURE .1

Figure S1. (A)Total cell lysates of PI4KIIα, PI4KIIβ, GAPDH and control siRNA-transfected HeLa cells were analysed by western blot using antibodies specific for the specified proteins. (B)HeLa cells were analysed for protein expression by western blotting; α-tubulin served as a control for protein levels. (C)Rescue of siRNA in HeLa cells. Western blots show loss and re- expression of siRNA-resistant recombinant PI4KIIα and PI4KIIβ following siRNA-mediated depletion. Asterisk indicates a proteolytic fragment resulting from the overexpression of GFP-PI4KIIα. (D) Confocal images

showing expression of siRNA resistant GFP-tagged PI4KIIα and HA-tagged PI4KIIβ, Scale Bars, 10 μM. (E and F)Confocal images showing immunostaining for phospho-tyrosines (red) and F-actin (green) following siRNA mediated silencing with or without transfection with siRNA resistant constructs.Data are presented as mean ± SEM, *; p<0.05, **; p<0.01, ***; p<0.001; ns, not significant.

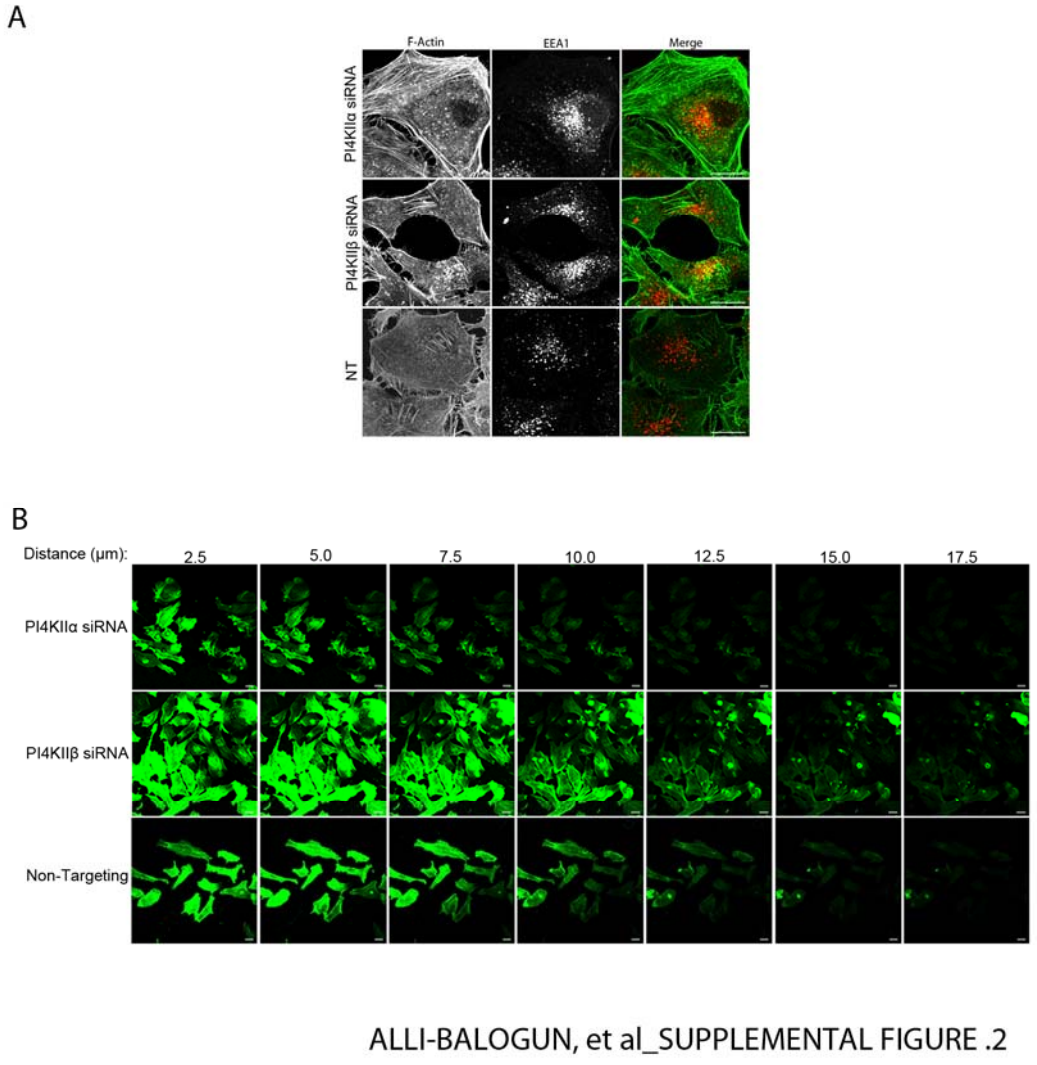

Figure S2.(A)Confocal images showing that scattered actin punctae induced upon PI4KIIβ depletion do not contain the endosomal marker EEA1. (B)Migration of siRNA treated cells via collagen-coated Transwell inserts towards a chemoattractant. Transwell membranes were coated with 100 μl type 1 collagen (2 mg/ml) gel. After staining with

Alexa-488 labelled phalloidin, fixed cells were visualised by confocal microscopy. Optical sections were acquired at 2.5 µm apart and are shown side by side with increasing depth.

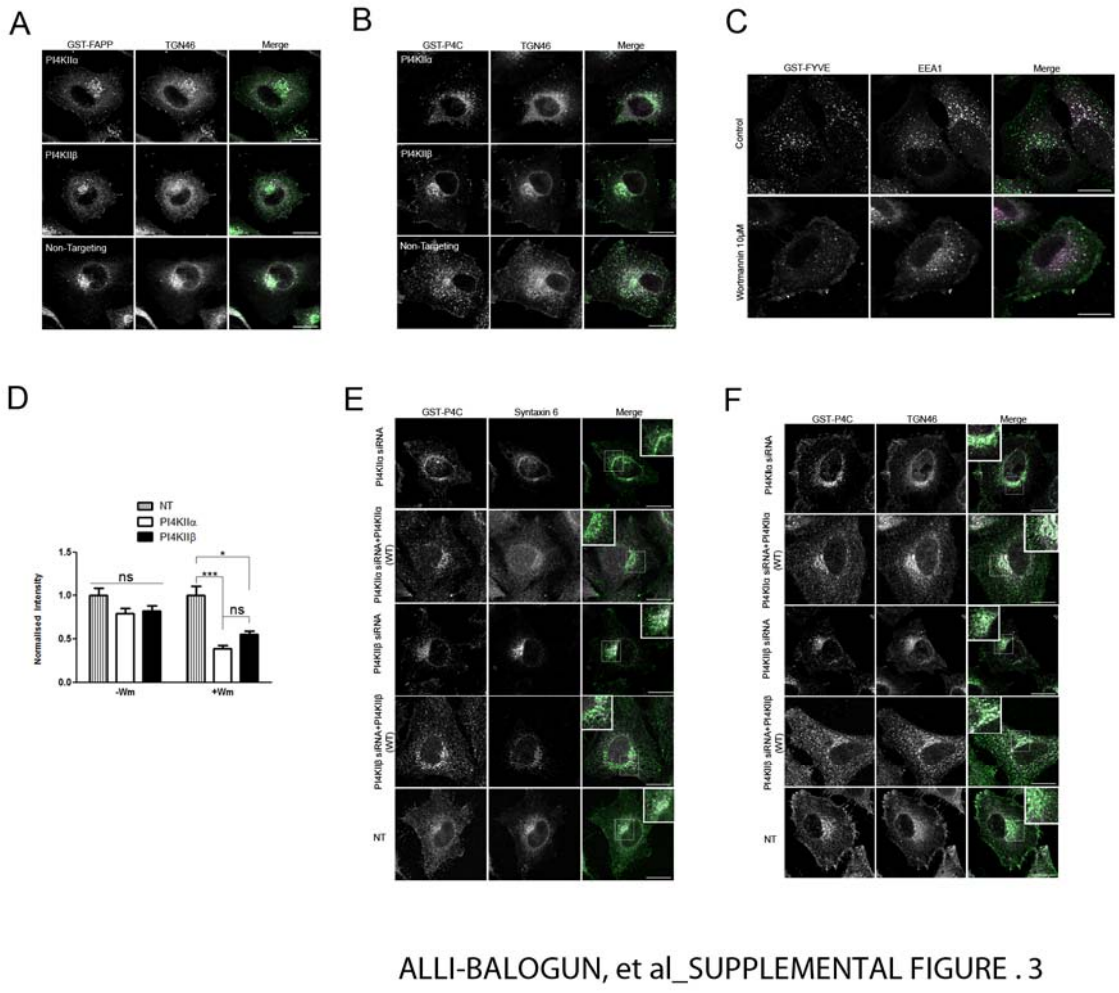

ALLI-BALOGUN, et al_SUPPLEMENTAL FIGURE . 3

Figure S3. (A)A recombinant GST-fusion of the PH domain of FAPP1 (GST-PH-FAPP1) was used to indirectly stain membrane pools of PI(4)P. Samples were co-immunostained with TGN46(B)Recombinant GST-tagged protein containing the P4C domain from the *Legionella pneumoniae*SidC protein (GST-P4C) was used to indirectly stain membrane pools of PI(4)P in the absence of wortmannin. (C)The ability of 10 µMwortmannin to inhibit PI 3-kinases was confirmed by probing fixed cells with GST-

tagged FYVE domain of Hrs (GST-2X-FYVE^{Hrs}). Cells were co-immunostained with early endosome marker, EEA1.(D)Quantification of staining of membrane pools of PI(4)P identified by GST-P4C after treatment with 10μM wortmannin.(E and F) Confocal images showing immunostaining for GST-P4C (green) and syntaxin 6 or TGN46 (magenta) following siRNA mediated silencing with or without rescue with siRNA-resistant constructs.Data are presented as mean ± SEM, *; $p<0.05$, **; $p<0.01$, ***; $p<0.001$; ns, not significant.

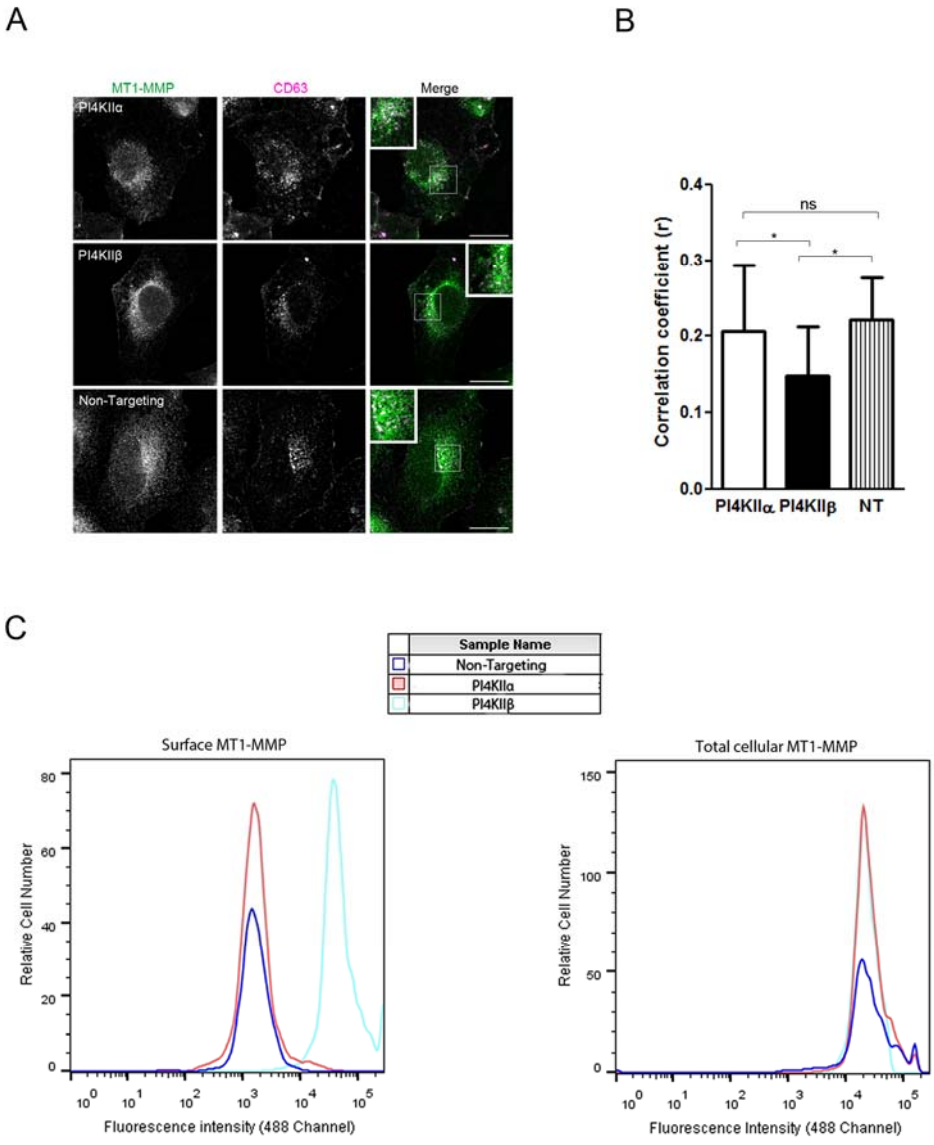

ALLI-BALOGUN, et al_SUPPLEMENTAL FIGURE .4

Figure S4. (A)Immunofluorescent staining of MT1-MMP and the lysosomal marker, CD63**.** (B)Pearson's correlation coefficients were calculated for co-localised pixels between MT1-MMP (green) and CD63 (magenta) channels. (C)Surface (unpermeablised cells) and total cellular (permeabilised with 0.05% Triton X-100) MT1-MMP levels were analysed by flow cytometry. Data are presented as mean ± SEM, *; $p<0.05$, **; $p<0.01$, ***; $p<0.001$; ns, not significant.

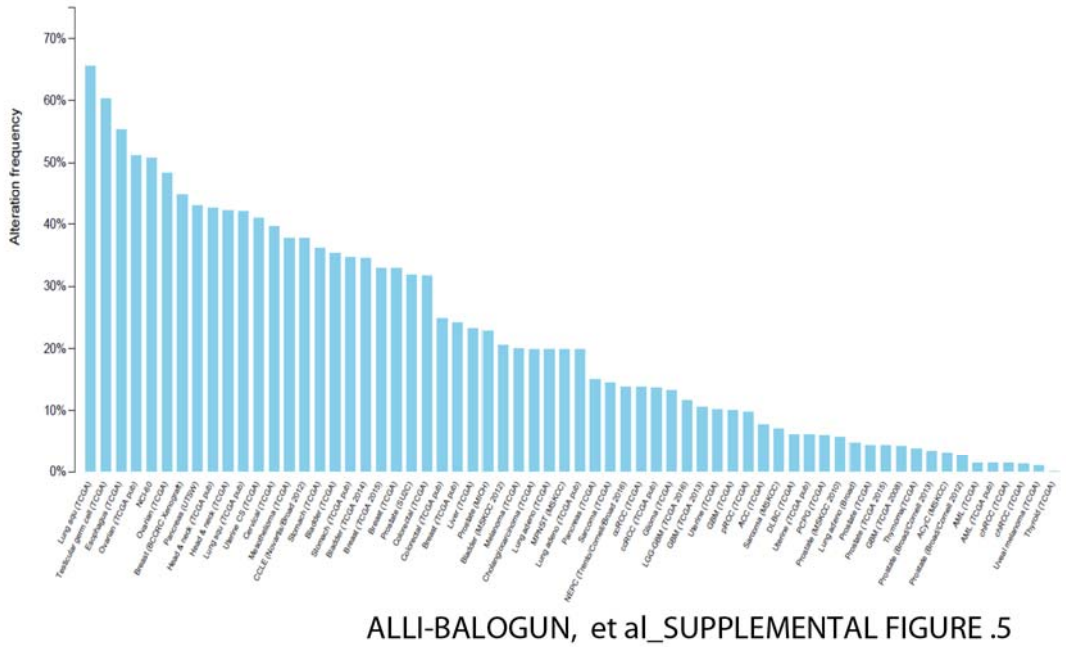

Figure S5. Cross cancer histogram showing heterozygous loss of PI4K2B across all cancer types. CBio Database analysis.

Supplemental references

Balla, T., Downing, G. J., Jaffe, H., Kim, S., Zolyomi, a., and Catt, K. J. (1997). Isolation and Molecular Cloning of Wortmannin-sensitive Bovine Type III Phosphatidylinositol 4-Kinases. J. Biol. Chem. *272*, 18358–18366.

Bolte, S., and Cordelières, F. P. (2006). A guided tour into subcellular colocalization analysis in light microscopy. J. Microsc. *224*, 213–232.

Bowden, E. T., Coopman, P. J., and Mueller, S. C. (2001). Invadopodia : Unique Methods for Measurement of Extracellular Matrix Degradation in Vitro. Methods Cell Biol. *63*, 613–627.

Hammond, G. R. V, Schiavo, G., and Irvine, R. F. (2009). Immunocytochemical

techniques reveal multiple, distinct cellular pools of PtdIns4P and PtdIns(4,5)P(2). Biochem. J. *422*, 23–35.

Mössinger, J., Wieffer, M., Krause, E., Freund, C., Gerth, F., Krauss, M., and Haucke, V. (2012). Phosphatidylinositol 4-kinase IIα function at endosomes is regulated by the ubiquitin ligase Itch. EMBO Rep. *13*, 1087–1094.

Simons, J. P. *et al.* (2009). Loss of phosphatidylinositol 4-kinase 2alpha activity causes late onset degeneration of spinal cord axons. Proc. Natl. Acad. Sci. U. S. A. *106*, 11535–11539.

Wieffer, M. *et al.* (2013). PI4K2β/AP-1-Based TGN-Endosomal Sorting Regulates Wnt Signaling. Curr. Biol. *23*, 2185–2190.